Lithos 354–355 (2020) 105323

Contents lists available at ScienceDirect

Lithos

journal homepage: www.elsevier.com/locate/lithos

Research Article

The role of water and compression in the genesis of alkaline basalts: Inferences from the Carpathian-Pannonian region

I. Kovács [a,b,*], L. Patkó [a,c,d], N. Liptai [a], T.P. Lange [a,c], Z. Taracsák [a,e], S.A.P.L. Cloetingh [b,f], K. Török [g], E. Király [g], D. Karátson [h], T. Biró [g], J. Kiss [h], Zs. Pálos [b], L.E. Aradi [c], Gy. Falus [c], K. Hidas [i], M. Berkesi [a,c], A. Koptev [j], A. Novák [a,b], V. Wesztergom [b], T. Fancsik [g], Cs. Szabó [b,c]

[a] MTA CSFK Lendület Pannon LitH$_2$Oscope Research Group, Sopron, Hungary
[b] CSFK Geodetic and Geophysical Institute, Sopron, Hungary
[c] Eötvös University, Department of Petrology and Geochemistry, Lithosphere Fluid Research Lab, Budapest, Hungary
[d] Institute for Nuclear Research, Isotope Climatology and Environmental Research Centre, Debrecen, Hungary
[e] University of Manchester, Department of Earth and Environmental Sciences, Manchester, UK
[f] Utrecht University, Tectonics Research Group, Utrecht, Netherlands
[g] Mining and Geological Survey of Hungary, Budapest, Hungary
[h] Eötvös University, Department of Physical Geography, Budapest, Hungary
[i] Instituto Andaluz de Ciencias de la Tierra, CSIC-UGR, Granada, Spain
[j] University of Tübingen, Department of Geosciences, Tübingen, Germany

ARTICLE INFO

Article history:
Received 2 June 2019
Received in revised form 25 November 2019
Accepted 4 December 2019
Available online 10 December 2019

Keywords:
Alkaline basalts
Carpathian-Pannonian region
Asthenosphere
Lithosphere
Deformation
Melting
Water

ABSTRACT

We present a new model for the formation of Plio-Pleistocene alkaline basalts in the central part of the Carpathian-Pannonian region (CPR). Based on the structural hydroxyl content of clinopyroxene megacrysts, the 'water' content of their host basalts is 2.0–2.5 wt.%, typical for island arc basalts. Likewise, the source region of the host basalts is 'water' rich (290–660 ppm), akin to the source of ocean island basalts. This high 'water' content could be the result of several subduction events from the Mesozoic onwards (e.g. Penninic, Vardar and Magura oceans), which have transported significant amounts of water back to the upper mantle, or hydrous plumes originating from the subduction graveyard beneath the Pannonian Basin.

The asthenosphere with such a relatively high 'water' content beneath the CPR may have been above the *'pargasite dehydration'* (<90 km) or the *'nominally anhydrous'* (>90 km) solidi. This means that neither decompressional melting nor the presence of voluminous pyroxenite and eclogite lithologies are required to explain partial melting.

While basaltic partial melts have been present in the asthenosphere for a long time, they were not extracted during the syn-rift phase, but were only emplaced at the onset of the subsequent tectonic inversion stage at ~8–5 Ma. We propose that the extraction has been facilitated by evolving vertical foliation in the asthenosphere as a response to the compression between the Adriatic indenter and the stable European platform. The vertical foliation and the prevailing compression effectively squeezed the partial basaltic melts from the asthenosphere. The overlying lithosphere may have been affected by buckling in response to compression, which was probably accompanied by formation of deep faults and deformation zones. These zones formed conduits towards the surface for melts squeezed out of the asthenosphere.

This implies that basaltic partial melts could be present in the asthenosphere in cases where the bulk 'water' content is relatively high (>~200 ppm) at temperatures exceeding ~1000–1100 °C. These melts could be extracted even under a compressional tectonic regime, where the combination of vertical foliation in the asthenosphere and deep fractures and deformation zones in the folded lithosphere provides pathways towards the surface. This model is also valid for deep seated transpressional or transtensional fault zones in the lithosphere.

1. Introduction

The genesis of the Plio-Pleistocene alkaline basalts in the Carpathian-Pannonian region (CPR) is still a controversial topic. This is mainly because the paroxysm of alkaline basaltic volcanic activity

* Corresponding author at: MTA CSFK Lendület Pannon LitH$_2$Oscope Research Group, Sopron, Hungary.
E-mail address: kovacs.istvan.janos@csfk.mta.hu (I. Kovács).

https://doi.org/10.1016/j.lithos.2019.105323

(~ 5–2 Ma) post-dated the main phase of extension (~17–11 Ma) in the CPR. The latter phase was not associated with this type of volcanic activity, instead massive areal calc-alkaline magmatism took place at this time (Horváth, 1993; Horváth et al., 2006, Seghedi et al., 2004; Pécskay et al., 2006; Szakács et al., 2018). The extension is generally considered capable of producing basaltic melts due to decompressional melting (e.g. Embey-Isztin et al., 1993). The timing of the onset of alkaline basaltic volcanic activity is enigmatic, coinciding with the collision of the main tectonic units with the stable European platform in the Carpathian embayment at ~11 Ma (e.g. Matenco et al., 2003). This means that the onset of alkaline basaltic volcanic activity generally took place in the post-rift phase after the cessation of extension and active subduction along the Carpathians. Even more interestingly, the paroxysm of alkaline basaltic volcanic activity is coeval with the onset of tectonic inversion in the CPR at ~8–5 Ma (e.g. Bada et al., 2007; Balázs et al., 2016). Consequently, alkaline basalts were produced mainly in a compressional tectonic regime, which is usually considered unfavourable for basalt genesis.

Volatiles, especially 'water' (if not otherwise specified, the term 'water' refers to all hydrous species in rocks: H^+, OH^- and H_2O), have an unprecedently large impact on the physical properties of rocks and melts at temperatures and pressures typical for the upper mantle (i.e., conductivity, anisotropy, effective viscosity and seismic velocity, see Kovács et al., 2018 for a review). In this paper within the term 'water', we also distinguished structural hydroxyls, which are hydrogen ions (H^+) attached to oxygens occupying different crystallographic sites in nominally anhydrous minerals (referred to as NAMs for short) forming hydroxyl groups. Note that both the 'water' and structural hydroxyl concentrations in melts and NAMs are expressed in molecular water (H_2O) equivalent either in ppm (wt.) or wt.%. respectively.

In particular, 'water' significantly lowers the solidus temperature of upper mantle peridotites (Green et al., 2010). However, such information on the concentration of 'water' in the asthenospheric source of alkaline basalts in the CPR is not yet available (e.g. Harangi et al., 2015; Seghedi et al., 2004). Consequently, without this piece of information it may be rather challenging to understand why partial melting could have occurred in the upper mantle. Recent findings have demonstrated that at depths shallower than 100 km (~3 GPa) of the upper mantle the solidus is the *'pargasite dehydration solidus'* at ~1050–1150 °C (~150 °C lower than previously anticipated) (Kovács et al., 2017) even at very low bulk 'water' contents (~200 ppm) typical for the MORB upper mantle (Dixon et al., 1988; Saal et al., 2002). This is due to the stability of pargasitic amphibole even at such low bulk 'water' concentrations (Green et al., 2010, 2014; Kovács et al., 2012a, 2017). At deeper levels in the upper mantle (>90 km), the solidus temperature is mainly controlled by the concentration of structural hydroxyl in NAMs among other variables such as pressure, oxygen fugacity and bulk composition. The effect of structural hydroxyls on the solidus can be taken into account by different melting models (Hirschmann et al., 2009; Katz et al., 2003). These models seem to be consistent in the sense that the depression of the solidus temperature with respect to the dry solidus is ~150 °C lower when there is ~500 ppm bulk structural hydroxyl in the upper mantle peridotite. The presence of pyroxenite and eclogite lithologies in the upper mantle are also known to lower the solidus temperature with respect to the *'dry solidus'* (e.g. Hirschmann and Stolper, 1996; Lambart et al., 2016; Rosenthal et al., 2014). So far, however, no detailed quantitative analysis has been undertaken to estimate the contribution of such lithologies to melting in the asthenosphere.

The two main goals of our study are:

(1.) To provide the first estimate on the structural hydroxyl content in the source region of alkaline basalts from the Bakony – Balaton Highland Volcanic Field (BBHVF) in the central CPR. To this purpose, the structural hydroxyl content of co-genetic clinopyroxene megacrysts was analysed by micro-FTIR spectrometry. From this, the 'water' content of the host basaltic melt and its source region is approximated using experimentally determined partition coefficients and the empirically constrained degree of partial melting (see Xia et al., (2013) for the details of the applied methodology).

(2.) Assuming that melt is present in the asthenosphere, a model is presented for how and why this melt was extracted from the asthenosphere in the tectonic inversion/compressional stage of the CPR. Regional seismic anisotropy data, lattice preferred orientation of upper mantle xenoliths, the concept of lithospheric-scale folding, the direction of geomagnetic induction vectors and focal mechanisms of earthquakes in the central Pannonian Basin provide additional support for the model.

In addition, we quantitatively estimate the contribution of pyroxenite and eclogite lithologies to the formation of alkaline basaltic melts in the upper mantle using bulk major and trace element compositions of alkaline basalts in the CPR with a focus on 'fingerprint' elements such as Mn, Fe, Zn, Co, and Ni (Le Roux et al., 2011).

2. Geological background and previous models for alkaline basaltic volcanic activity in the CPR

A brief overview on the genesis of Plio-Pleistocene alkaline basalts in the CPR is provided below, as this topic has been covered in great detail in previous studies (e.g. Ali et al., 2013; Ali and Ntaflos, 2011; Embey-Isztin et al., 1993; Harangi et al., 2015; Kereszturi et al., 2010, 2011; Németh et al., 2001; Seghedi et al., 2004; Szabó et al., 1992). The following main alkaline basaltic volcanic fields are located in the CPR from west to east: Styrian Basin (SBVF); Burgenland; Little Hungarian Plain (LHPVF); Bakony–Balaton Highland (BBHVF); Nógrád-Gömör (NGVF) and Perşani Mts. (PMVF) (Fig. 1). In these volcanic areas basaltic pyroclastic successions (Szentbékkálla, BBHVF) and effusive basalts building up lava plateaus (Medves, NGVF) or small shield volcanoes (Kab Mt., BBHVF) occur as well. Furthermore, there are several smaller isolated occurrences of alkaline basalts in the CPR at Kecel, Štiavnica and Lucareţ. The basaltic activity started at ~11 Ma at the western margins of the CPR (Burgenland) and lasted till sub-recent times at Štiavnica (few hundred ka; Balogh et al., 1981; Chernyshev et al., 2013) with the main phase of volcanism taking place between 5 and 2 Ma (Pécskay et al., 2006; Wijbrans et al., 2007). Since the PMVF is generally younger than the other localities (<2 Ma) and situated on a geodynamically distinct part of the CPR outside the Pannonian Basin (e.g. Harangi et al., 2013; Seghedi et al., 2004, 2016), its detailed investigation is beyond the scope of our study.

The earliest models (e.g. Embey-Isztin et al., 1993; Szabó et al., 1992) proposed that the basaltic activity was generated in the post-extensional phase during the period of thermal relaxation. The thermal relaxation led to the cooling and contraction of the asthenospheric dome creating deep fractures in the overlying lithosphere, which channelled melts from the partially molten asthenosphere to the surface. While this model seems to provide a reasonable explanation for how the melt may have been extracted from the asthenosphere, it fails to explain why and how partial melting occurred in the cooling asthenospheric dome. In addition, it is difficult to reconcile how deep fractures were 'opened up' in the subsiding lithosphere over the thermally shrinking asthenospheric dome in a compressional tectonic regime when both the lithosphere and asthenosphere were under compression between the Adriatic indenter and the stable European platform.

In subsequent papers, Wilson and Downes (2006) and Seghedi et al. (2004) argued that deep thermal plume fingers may exist under the major volcanic fields in the CPR. This scenario was ruled out by Harangi and Lenkey (2007) and Harangi et al. (2015). Their studies demonstrated that the upper mantle beneath the volcanic fields is thermally not anomalous (i.e. shows potential temperatures typical for ambient mantle: ~1300–1450 °C) which is at least 100 °C lower than what

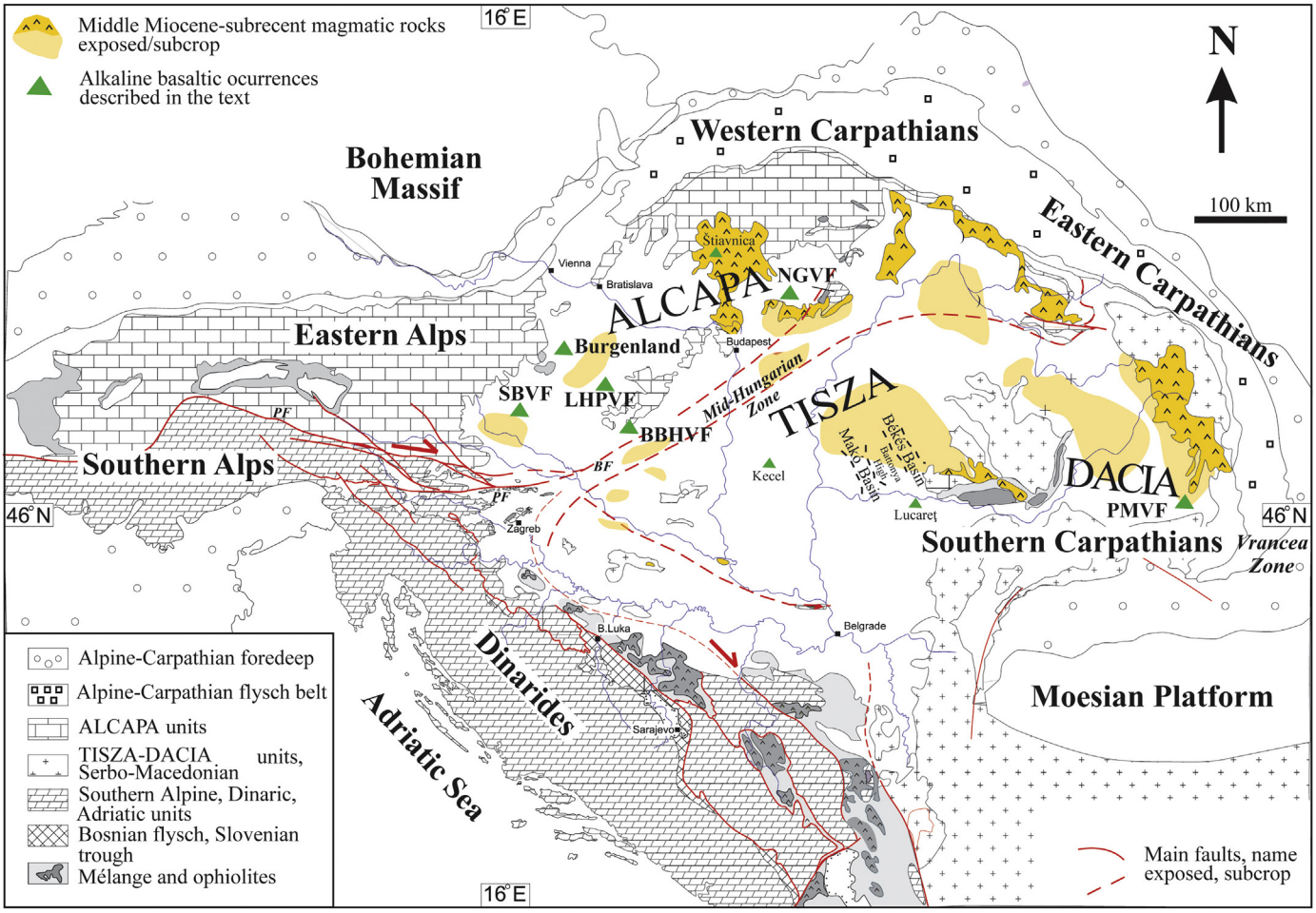

Fig. 1. Schematic geological map of the Carpathian-Pannonian region (CPR) with location of main alkaline basaltic localities (BBHVF: Bakony-Balaton Highland Volcanic Field; LHPVF: Little Hungarian Plain Volcanic Field; NGVF: Nógrád-Gömör Volcanic Field; PMVF: Perşani Mts. Volcanic Field; SBVF: Styrian Basin Volcanic Field). The map is modified after Kovács et al. (2012b). Abbreviations for major faults are (with bold italic): PF – Periadriatic fault, BF – Balaton fault.

would be considered characteristic for mantle plumes (e.g. Green and Falloon, 2005). As recently shown by seismic tomography, there is a 'graveyard' of subducted slabs beneath the CPR (Dando et al., 2011; Hetényi et al., 2009) where remnants of previously subducted rocks are accumulated at the mantle transition zone between ~410 and ~660 km. This also makes the existence of deep-rooted thermal plume (s) (fingers) rather unlikely beneath the CPR, as plumes would first have to penetrate these slab remnants before rising to the shallower levels of the upper mantle. During the last decade, seismic tomography has provided increasing evidence for the existence of 'baby plumes' rising from depth levels from 670 to 440 km in the upper mantle underlying western and central Europe (Ritter and Christensen, 2007).

Harangi et al. (2015) has recently proposed that asthenospheric flow could also be responsible for melting in the asthenosphere beneath the CPR. In their model, asthenospheric flow is induced at locations where the lithosphere-asthenosphere boundary is steep by 'thin spot' suction of the extending lithosphere. The thinned lithosphere exerts suction on the ambient asthenosphere and promotes its flow into the CPR from beneath the surrounding areas, especially from the Alps and the Bohemian Massif. These authors point out that this flow might occur in particular along the relatively steep lithosphere-asthenosphere boundary at the western and northern edges of the CPR. The driving force for melting is assumed to be decompression in the uprising asthenosphere. This model, however, raises several questions concerning space and time. Most importantly, there is obviously a problem with the timing as the main phase of the extension (syn-rift phase) in the southwestern and eastern part of the CPR ceased at ~11 and ~8 Ma, respectively (Horváth et al., 2006; Márton and Fodor, 2003). The paroxysm of the alkaline basaltic volcanic activity in the CPR occurred ~5–2 Ma, which is considerably younger than the supposed 'thin spot' suction generated by the thinning of the lithosphere. During 'thin spot' suction the extension of the lithosphere and the uprise of the underlying asthenosphere should be simultaneous. While this 'thin spot' model was argued to account for the formation of all but the PMVF basalts, there are alkaline basalts in the LHPVF and BBHVF (and smaller occurrences in the central Pannonian Basin) (Fig. 1), which are distant from locations with a steep lithosphere-asthenosphere boundary (LAB, Horváth, 1993). It follows that even if the 'thin' spot model was true, it would fail to explain the genesis of alkaline basalts in these central locations where the LAB is relatively flat. It is possible, however, that the formation of the oldest alkaline basalts in Burgenland where the syn-rift stage was almost coeval with the timing of the eruptions and where the lithosphere-asthenosphere boundary is indeed steep, may be explained by this 'thin spot' model.

Further uprising of the asthenosphere following the syn-rift stage also seems unlikely. In fact, it is more probable that following the syn-rift stage the lithosphere may have started thickening immediately as the asthenospheric dome began to cool. During this thermal relaxation, the uppermost part of the asthenospheric dome was gradually converted into new and juvenile lithosphere. This 'lithospherisation' process is discussed in detail by Kovács et al. (2012b, 2017) and its main driving force is that at lower temperatures (<1050 °C) the pargasitic amphibole becomes a stable mineral phase in the upper mantle. This hydrous chain silicate (containing ~2 wt.% H_2O) lowers the activity of

'water' and incorporates free fluids and melts (Green et al., 2010, 2014; Kovács et al., 2012a, 2017). The consequent (partial) disappearance of fluids and melts (e.g. Berkesi et al., 2019) and the decreasing solubility of structural hydroxyl in NAMs of the upper mantle (Kang et al., 2017) both increase the effective viscosity of the upper mantle, making it rheologically stronger (e.g. Dixon et al., 2004; Li et al., 2008). Thus, the thermal relaxation following the main phase of extension is not favourable for melt formation and preservation in the cooling asthenospheric dome. Based on upper mantle peridotite xenoliths, Kovács et al. (2012b) concluded that in the central part of the CPR (BBHVF), the lithosphere may have thickened from its 'original' 40 km thickness at the end of the syn-rift stage to ~60 km at the time of the alkaline basaltic volcanic activity.

In summary, previous models do not appear to provide a comprehensive and self-consistent explanation for the genesis of Plio-Pleistocene alkaline basalts in the CPR, raising the need for alternative explanations. Key questions remain on the cause for melting in the asthenosphere and on the mode of melt extraction. Below we present a new conceptual model based on the estimated 'water' content in the asthenospheric source of alkaline basalts and deformation in the lithosphere-asthenosphere system during the tectonic inversion stage of the CPR.

3. Constraining the 'water' content in the source of alkaline basalts from the BBHVF

3.1. Selecting suitable samples

In recent years it has become a common practice to estimate the 'water' content in the source region of alkaline basalts based on the structural hydroxyl content in their co-genetic and geochemically primitive clinopyroxene megacrysts (e.g. Liu et al., 2015; Xia et al., 2013). It is widely accepted that these clinopyroxenes form at the very early stage of crystallization, and consequently they are expected to be in equilibrium with pristine, near liquidus basaltic melts. Demouchy et al. (2006) and Peslier and Luhr (2006) demonstrated that basaltic melts usually reach the surface within a few tens of hours, and, thus, if the size of the megacrysts is large the chance for structural hydroxyl loss is limited. The size of the selected megacrysts is several centimetres in diameter.

In our present study, the structural hydroxyl concentrations of 5 clinopyroxene megacrysts from Szentbékkálla and Szigliget (both from BBHVF) reported by Kovács et al. (2016) were found to be suitable for this methodology from a larger pool of available megacrysts. These clinopyroxenes are primitive enough in composition (high mg#: >0.75) and display no chemical zonation or any evidence for syn- or post-eruptive structural hydroxyl loss. Liu et al. (2015) demonstrated, based on modelling of magma evolution, that clinopyroxenes with mg# higher than 0.75 can still be a relatively reliable source of information (within 30%) for the host magma regarding its original 'water' content. In addition, primitive mantle (PM) normalised trace element patterns of the selected clinopyroxenes in the rare earth element (REE) (Fig. 2a) and spider (Fig. 2b) diagrams are very similar to colourless megacrysts described for the BBHVF by Jankovics et al. (2016). All clinopyroxenes show enrichment in light and middle REE with respect to the heavy REE (Fig. 2a), and light REE are relatively depleted compared to middle REE. In the spider diagram (Fig. 2b), clinopyroxenes are mostly depleted in Ba, Th, Nb, Pb and Cr with respect to the PM and show negative anomalies for Ba, Nb, Pb, Sr, Zr and Cr. Jankovics et al. (2016) argued that the colourless megacryst is the early product of fractional crystallization representing a near-liquidus phase.

In addition, the selected clinopyroxenes also show similarity in the REE and spider diagrams (Fig. 2) to some clinopyroxenes from cumulates (Kovács et al., 2004) and clinopyroxene megacrysts in alkaline basalts from the NGVF (Dobosi and Jenner, 1999). The latter are also interpreted to represent products of very early stage fractional crystallisation. These latter samples, however, sometimes display slightly higher trace element concentrations than those from the BBHVF. Furthermore, the light REE are not or only slightly depleted compared to middle REE (Fig. 2a) and Th and U are considerably enriched (Fig. 2b).

In Kovács et al. (2016), all but the 'Szigliget cpx1' clinopyroxene have high mg# (>75) indicating that they are primitive in composition and in equilibrium with the host basalt in the early stage of its crystallisation. 'Szigliget cpx1' has, however, much lower mg# (~58) and its structural hydroxyl content is also lower (285 ppm). This implies that this clinopyroxene might have formed in a more advanced stage in the evolution of the basaltic magma, by which time the melt may have suffered some degassing. For this reason, only clinopyroxenes with higher mg# (76–81) were selected for the calculation of the 'water' content of the primitive basaltic melts (e.g. Chen et al., 2015, 2017; Liu et al., 2015). Among the samples with sufficiently high mg#, however, clinopyroxene samples from the Kapolcs locality were also omitted because of their appreciably lower structural hydroxyl contents and anomalous infrared spectra. The lower structural hydroxyl concentration and the anomalous infrared spectra (see Fig. 1 in Kovács et al., 2016) may refer to pre-, syn- or post-eruptive modification of the original structural hydroxyl contents of clinopyroxenes in equilibrium with their host alkaline basalts (Patkó et al., 2019) which could be due to several factors including decreasing 'water' activity, annealing or oxidation. In case of the Kapolcs clinopyroxenes, the annealing at low 'water' activity appears to be the most plausible explanation as these crystals are originated from basaltic lava rocks, whereas those from Szigliget and Szentbékkálla are from basaltic pyroclasts (e.g. Jankovics et al., 2012). This means that the Kapolcs lava rocks may have cooled more slowly staying at higher temperatures for a longer period of time which may have facilitated to reach equilibrium quicker at low 'water' activities (Lloyd et al., 2016). Absorption bands correspond to different substitution mechanisms of structural hydroxyl into clinopyroxene which all have their characteristic stoichiometry (e.g. Tollan et al., 2017 for olivine). As different stoichiometries do have different dependences on water activity, this also affects the relative contributions of the different bands in NAMs with changing water activity. Clinopyroxenes displaying their maximum absorption bands at the higher and lower wavenumbers are typical for higher and lower 'water' activity, respectively (Patkó et al., 2019). Consequently, clinopyroxenes crystallised in the early stage of fractional crystallisation at high pressure (and therefore higher 'water' activity prior to significant degassing) should have their maximum bands at the highest wavenumbers, whereas for those crystallised later at lower pressure or after considerable degassing the maximum band is expected to appear at lower wavenumber.

The two clinopyroxenes from Kapolcs have only 97–112 ppm of structural hydroxyl, whereas those selected from Szentbékkálla and Szigliget are in the range of 391–476 ppm (see Table 1 in Kovács et al., 2016). In addition, in the Kapolcs clinopyroxenes, the intensity of the 3520 cm^{-1} absorption band is predominant, whereas the 3625 cm^{-1} band is almost invisible. This is in contrast with the 'general' trend shown by other clinopyroxenes in equilibrium with their environment, where the ~3630 cm^{-1} band is the most intensive and the other bands at lower wavenumbers show gradually lower absorbance (Aradi et al., 2017; Bonadiman et al., 2009; Ferriss et al., 2016; Kovács et al., 2012a; Pintér et al., 2015; Sundvall and Stalder, 2011; Weis et al., 2015).

In summary, great care must be taken when selecting suitable clinopyroxene grains for estimating the 'water' content in their equilibrium basaltic melt. The geochemistry, infrared spectra and structural hydroxyl content of clinopyroxenes, as well as their pre- and post-eruptive history must be examined to ensure that their structural hydroxyl concentration represents equilibrium conditions with their host melt. The structural hydroxyl contents of clinopyroxenes are determined from unpolarised micro-FTIR spectrometry (see Kovács et al., 2016 for details of the analytical technique) and are accurate within

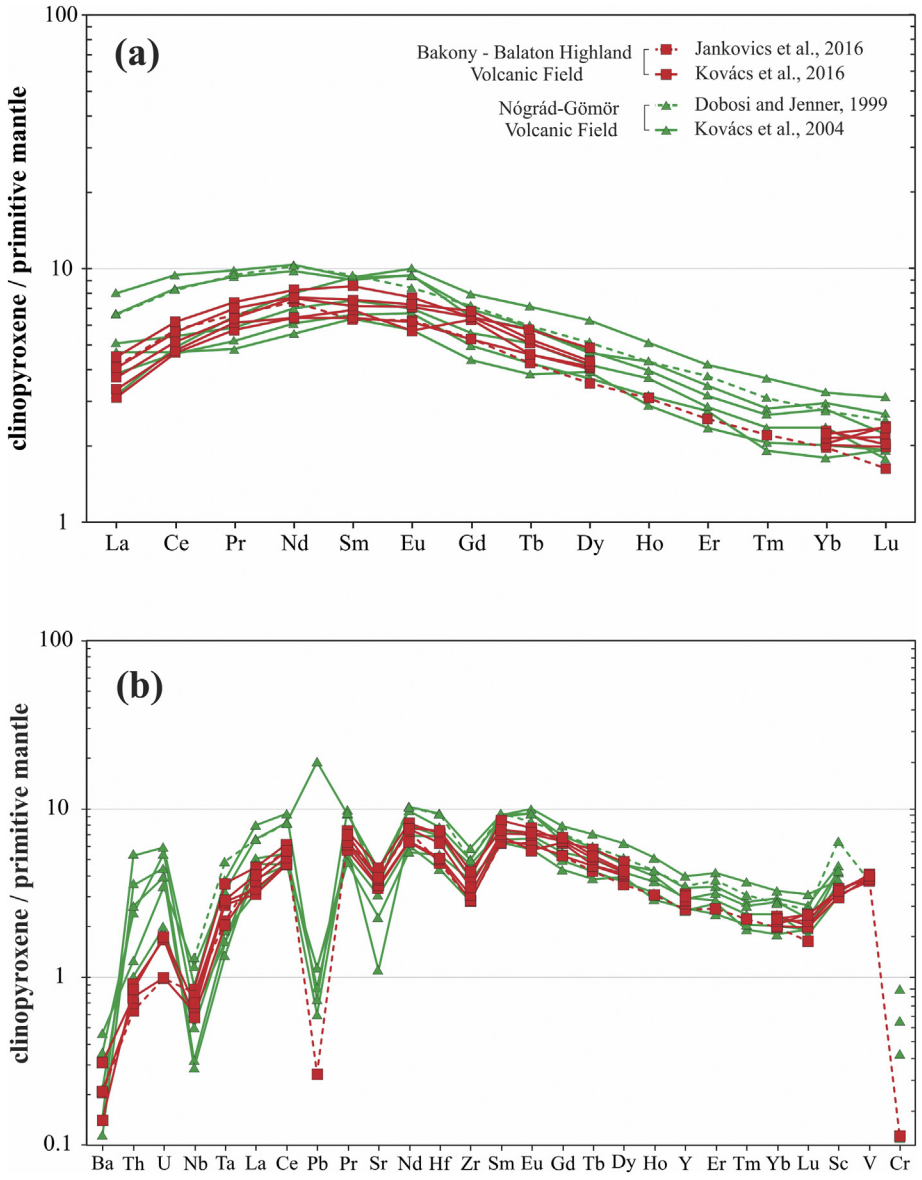

Fig. 2. Rare Earth Element (REE) (a) and spider (b) diagrams for clinopyroxene megacrysts from the BBHVF (Jankovics et al., 2016) and NGVF (Dobosi and Jenner, 1999) and clinopyroxenes from Type-II cumulate xenoliths from the NGVF (Kovács et al., 2004) all hosted in alkaline basalts. For comparison, the compositions of the studied clinopyroxenes from Kovács et al. (2016) are also highlighted. The diagrams are all normalised to primitive mantle composition based on Sun and McDonough (1995).

15% (Table 1). The measured concentration range defined by the suitable clinopyroxenes from Szentbékkálla and Szigliget is rather narrow from 391 to 476 ppm implying homogenous 'water' concentration in their parental melt.

3.2. 'Water' content of the parental melt

In the second step, the 'water' content of the basaltic melt in equilibrium with the selected clinopyroxenes can be calculated using the composition dependent partition coefficient of O'Leary et al. (2010). The partition coefficient can be calculated using Equation (10) in O'Leary et al. (2010) which includes the $Al^{(IV)}$ and Ca cation fractions of clinopyroxenes and depends mainly on the $Al^{(IV)}$ content (Eq. 1):

$$\ln D_{H_2O}^{cpx-melt} = -4.2 + 6.5 \cdot X_{Al^{IV}}^{cpx} - 1 \cdot X_{Ca}^{cpx} \quad (1)$$

note that $Al^{(IV)}$ is calculated as (Eq. 2):

$$^{IV}Al^{3+} = \frac{1}{2}\left(\sum Al^{3+} - Na^{+}\right) \quad (2)$$

As partition coefficients do not depend strongly on pressure and temperature, abandoning these factors has only negligible effect on the partition coefficient. The cation numbers are calculated based on the major element compositions of clinopyroxenes provided in Table 1 (extracted from Supplementary Table 1 of Kovács et al., 2016). The determined $D_{H_2O}{}^{Cpx-melt}$ values range from ~0.018 to 0.020 (Table 1). With these partition coefficients, the 'water' content of the basaltic melt in equilibrium with the clinopyroxenes was calculated and the results vary between 2.0 and 2.5 wt.% (Table 1).

3.3. Effects of fractionation on parental melt 'water' contents

'Water' content in equilibrium with the clinopyroxene megacrysts can be modified by fractionation, which increases the 'water' content

Table 1
Parameters used to calculate the water content in the source region of alkaline basalts.

Clinopyroxene phenocrysts	Szigliget cpx2	Szigliget cpx3	Szentbékkálla cpx104	Szentbékkálla cpx1_0	Szentbékkálla cpx108	
X_{Ca}^{cpx} [a]	0.762	0.753	0.733	0.766	0.732	
$X_{Al^{IV}}^{cpx}$ [a]	0.158	0.156	0.154	0.150	0.154	
$D_{H_2O}^{cpx-melt}$	0.0195	0.0195	0.0196	0.0185	0.0196	
				max	min	
H_2O ppm wt. in cpx	476	396	473	455	391	
H_2O wt.% in basaltic melt	2.44	2.03	2.41	2.47	2.00	Average
Compensated for 15% fractionation				**2.10**	1.70	1.65
compensated for 40% fractionation				1.48	**1.20**	
H_2O ppm wt. in the source region:						
Batch melting[b]	400			660	380	**520**
Fractional melting[b]				510	290	**400**

Bold characters in the min and max columns of the table display the possile minimum and maximum H_2O content of the host basalt after 40 and 15% fractionation respectively. Bold characters in the average column mean the average 'water' content of the source for batch and fractional melting respectivel.

[a] Chemical compositions and water contents of clinopyroxenes are from Kovács et al. (2016). Cation numbers are calculated following the routine outlined in Table A5 of O'Leary et al. (2010).

[b] Water concentration in the source region is calculated by assuming either batch or fractional melting. The minimum degree of melting (f) for the Bakony–Balaton Highland is taken from Harangi et al. (2015) and it is f = 0.025±0.0075. The partition coefficient (D) between basaltic melt and its source rock is taken as the average from Aubaud et al. (2004), Hirschmann et al. (2009) and Tenner et al. (2009), and its value is 0.009 ± 0.004. The cumulative 2σ uncertainity in the calculated water contents is ~40% inlcuding all possible sources of unsureness (i.e. partition coeffecicients of water, degrees of partial melting, 'water' content of pyroxene phenocrysts).

of the melt if degassing does not occur at the same time. Therefore, using clinopyroxene-melt equilibrium 'water' contents can overestimate the 'water' content of the parental melt. As clinopyroxenes in this study cover a range of mg# values, they presumably represent the magmatic system after various degrees of crystallisation. To estimate the degree of fractionation required to produce clinopyroxenes with similar composition to those megacrysts, we performed isobaric fractionation modelling in rhyolite-MELTS 1.2.0 (Ghiorso and Gualda, 2015; Gualda et al., 2012). As starting composition, a primitive (mg#>0.66) whole-rock composition from Szigliget (SZ-651, Embey-Isztin et al., 1993) was used. The pressure was set at 1 GPa (equal to ~35 km depth, representative to the uppermost lithospheric mantle beneath the BBHFV), while the oxygen fugacity was set at FMQ+1.3. To estimate the 'water' content of the primitive melt, between 1.5 and 2.0 wt.% H_2O was added to the system.

Results are shown in Fig. 3. The MELTS model predicts two various clinopyroxene compositions: a diopside-poor one ($CaO/Al_2O_3 < 1.6$, $CaO < 7$ wt.%) and a diopsidic one ($CaO/Al_2O_3 > 1.8$; $CaO > 16$ wt.%; Fig. 3c). The latter provides a good match to the compositions of the clinopyroxene megacrysts. Furthermore, spinel is also predicted by MELTS to appear in the system. From a comparison of the mg# of the clinopyroxene megacrysts with the clinopyroxene compositions calculated in MELTS, the degree of fractionation can be estimated between ~15% for most Mg-rich crystals. In the case of the crystal with the lowest mg# (Szentbékkálla cpx104) this value is ~40% (Fig. 3a). After taking the effect of crystallization into account, parental magma 'water' contents can be estimated to be between 1.5 and 2 wt.% by MELTS (Fig. 3b). Note that if the 15 or 40% fractionation is taken into account for the estimations based on the structural hydroxyl content of clinopyroxene megacryst (i.e., 2–2.5 wt.%), the range defined by the minimum and maximum 'water' contents spans from 1.2 to 2.1 wt.%. This range agrees very well with estimates obtained from MELTS (i.e., 1.5–2 wt.%).

3.4. 'Water' content in the mantle source

The 'water' content of the mantle source region for the alkaline basalts can be calculated if bulk partition coefficients for 'water' between basaltic melts and their peridotitic sources are known, and if information is available on the degree of partial melting. The partition coefficient for 'water' between basaltic melts and their peridotitic source rock ($D_{H_2O}^{solid-melt}$) has been constrained by experimental and theoretical studies and is in the range between 0.005 and 0.013 (e.g. Aubaud et al., 2004; Hao et al., 2014; Hirschmann et al., 2009; Tenner et al., 2009).

The degree of partial melting for the BBHVF alkaline basalts was constrained by the critical melting model of Sobolev and Shimizu (1992) as parameterised in Harangi et al. (2015) using the trace element composition of bulk alkaline basalts from the CPR (Fig. 4). In Fig. 4, samples from the BBHVF fall mostly on or close to the trend defined by the partial melting of garnet-peridotite (see also figFig. 9 in Harangi et al., 2015). The degree of partial melting is between 2 and 3%, closer to the latter. In Fig. 4 the non-modal equilibrium partial melting model for the PMVF alkaline basalts as parameterised by Harangi et al. (2013) is also highlighted. The alkaline basalts from the BBHVF also fall on the garnet-lherzolite melting trend. However, the degree of partial melting in this case is higher and ranges between 3 and 5%. For the sake of simplicity we applied an average degree of partial melting within the broad range defined by earlier studies discussed above based on trace element modelling (f = 0.0225, i.e. 2.25% partial melting) and an average partition coefficient ($D_{H_2O}^{solid-melt}$=0.009) to calculate the 'water' content in the source region, which is a conservative approach providing estimates closer to the minimum.

Using modal batch (Eq. 3) or fractional (Eq. 4) melting models, the 'water' concentration in the source region can be calculated as follows:

$$C_0^{H_2O} = C_{melt}^{H_2O} \cdot (D + f \cdot (1 - D)) \quad (3)$$

$$C_0^{H_2O} = C_{melt}^{H_2O} \cdot f / \left(1 - (1 - f)^{1/D}\right) \quad (4)$$

For these calculations, fractionation corrected (taking into account the modelled degrees of fractionation between 15 and 40%; Table 1) minimum, maximum and average 'water' contents were adopted for the basaltic melts ($C_{melt}^{H_2O}$). The batch melting model gives 'water' concentrations which are higher than those obtained from the fractional melting model (Table 1). The batch melting model provides minimum and maximum 'water' contents of 380 and 660 ppm, respectively, whereas the fractional model results in values of 290 and 510 ppm, respectively. The 'average' water contents by the batch and fractional model are 520 ± 200 and 400 ± 150 ppm, respectively.

The calculated average 'water' content in the source increases both with the degree of partial melting and the increasing partition coefficient (i.e. more 'water' is partitioned into the solid phase). Accordingly, the source region would be the richest in 'water' (~700 and ~550 ppm

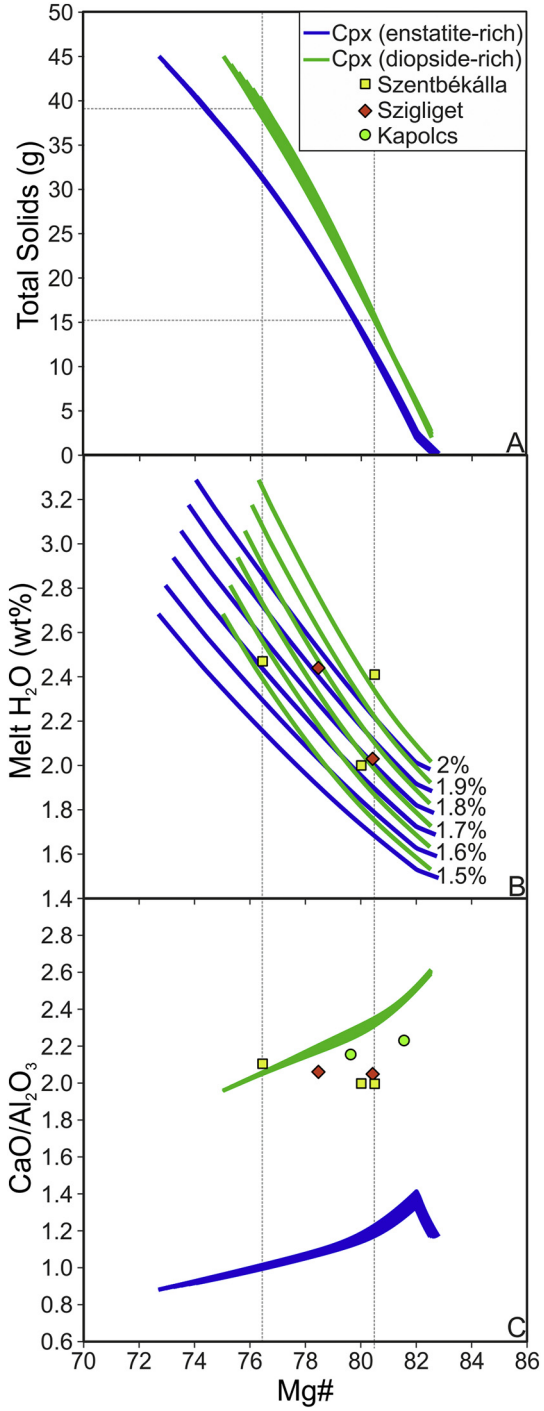

Fig. 3. Results of the isobaric crystallisation model carried out in rhyolite-MELTS 1.2.0 (Ghiorso and Gualda, 2015; Gualda et al., 2012) using whole-rock sample SZ-651 (Embey-Isztin et al., 1993) as a starting composition. The degree of fractional crystallisation vs. mg# number diagram (a) indicates clinopyroxenes with mg# = 76–82 are in equilibrium with liquids after ~15–40% fractionation. In (b), the change in 'water' contents as a function of mg# is shown, indicating that 'water' content of the melt steadily increases as the magma becomes more evolved. Melt 'water' contents of 2–2.4 wt% based on clinopyroxene megacrysts' structural hydroxyl concentrations can be derived from parental melts with 1.5–2 wt% H_2O. In (c) the major element composition of the two clinopyroxenes (blue: Ca-poor, clinoenstatite, green: Ca-rich, diopside) is shown: the studied crystals are a good match in both #mg range and CaO/Al_2O_3 ratio with the modelled diopsidic clinopyroxene compositions.

for modal batch and fractional melting respectively) if the degree of partial melting was ~3% and the partition coefficient was 0.013 (both values are at their maximum, although the degree of partial melting could be even higher). In contrast, there would be 'only' ~330 and 260 ppm 'water' (for modal batch and fractional melting respectively) in the source when the degree of partial melting was ~1.5% and the partition coefficient was 0.005. Thus we can argue that the minimum 'water' concentration in the source region is 260 ppm, but more likely in the average range between 400 and 520 ppm. For extreme parameters, 'water' contents could even reach values up to 700 ppm.

4. Discussion

4.1. Structural hydroxyl content of clinopyroxenes, 'water' content of their equilibrium basaltic melts and their source region

Clinopyroxenes show intermediate to high structural hydroxyl concentrations (391–476 ppm; Kovács et al., 2016) compared to the range defined by clinopyroxenes from upper mantle peridotite xenoliths, mega- and megacrysts from igneous rocks worldwide (e.g. Aradi et al., 2017; Bonadiman et al., 2009; Demouchy and Bolfan-Casanova, 2016; Denis et al., 2015; Hao et al., 2016; Kovács et al., 2012a; Patkó et al., 2019; Peslier et al., 2017; Pintér et al., 2015; Sundvall and Stalder, 2011; Xia et al., 2019).

We compared the fractionation corrected 'water' concentrations (1.2–2.1 wt.% assuming 40 and 15% fractionation, respectively) in the equilibrium basaltic melt with typical ranges for mid-ocean ridge basalts (<~0.5 wt.%; MORB), ocean island basalts (0.5–1.0 wt.%; OIB), back-arc basin basalts (0.5–2.0 wt.%; BABB) and island arc basalts (2.0–8.0 wt.%; IAB). From this it appears that they exceed those of MORB and OIB, but fall on the higher end of BABB and the lower end of IAB (Dixon et al., 2004; Xia et al., 2013). This concentration range represents intermediate to high values compared to those estimated for the Eastern Chinese alkaline basalts (Xia et al., 2013, 2019).

The 'water' content of the source regions has been estimated to be in the average range of 400–520 ppm after fractionation correction (Table 1). This range is significantly higher than what is typical for MORB (50–250 ppm, e.g., Dixon et al., 1988; Saal et al., 2002) and more in line with the estimates for OIB and E-MORB mantle source (300–1000 ppm, e.g. Dixon et al., 2002; Asimow et al., 2004). Therefore, we conclude that the asthenospheric source region of alkaline basalts beneath the CPR is considerably enriched in 'water' relative to MORB. In the next paragraph we present possible explanations for the 'wet' nature of the asthenosphere beneath the CPR.

4.2. Possible explanations for relatively 'water'-rich asthenosphere beneath the BBHVF

Prior to and partially during the Oligocene-Miocene extrusion of the Alcapa and Tisza-Dacia microplates (Fig. 1), the Carpathian embayment was surrounded by active subduction zones of oceanic or highly extended continental lithosphere (i.e. Balázs et al., 2016; Csontos and Vörös, 2004; Horváth et al., 2006, 2015; Schmid et al., 2008). These subductions may have been capable of transferring considerable amounts of volatiles back to the upper mantle beneath the CPR over geological times. The Penninic Ocean on the NE started subducting in the Mesozoic and its closure took place in the Eocene (Schmid et al., 2004). Almost simultaneously in the SW, the Vardar subduction may have transferred volatiles beneath the Carpathian embayment (Karamata, 2006). To the E and NE, the eastern continuation of the Penninic Ocean, the Magura Ocean started subducting in the Eocene (Oszczypko, 1992) and was closed by Late Miocene times (Kováč et al., 1994). Furthermore, on the western edge of the Pannonian Basin the Penninic subduction during the Eocene could have also affected the lithospheric mantle beneath the SBVF (Aradi et al., 2017). The time span of several tens of million years of continuous subduction below the Carpathian embayment must have been sufficiently long for extensive hydration of the overlying mantle wedge (Arcay et al., 2005, 2006; Gerya et al., 2002), and for allowing the subducting slabs to reach the 660 km discontinuity

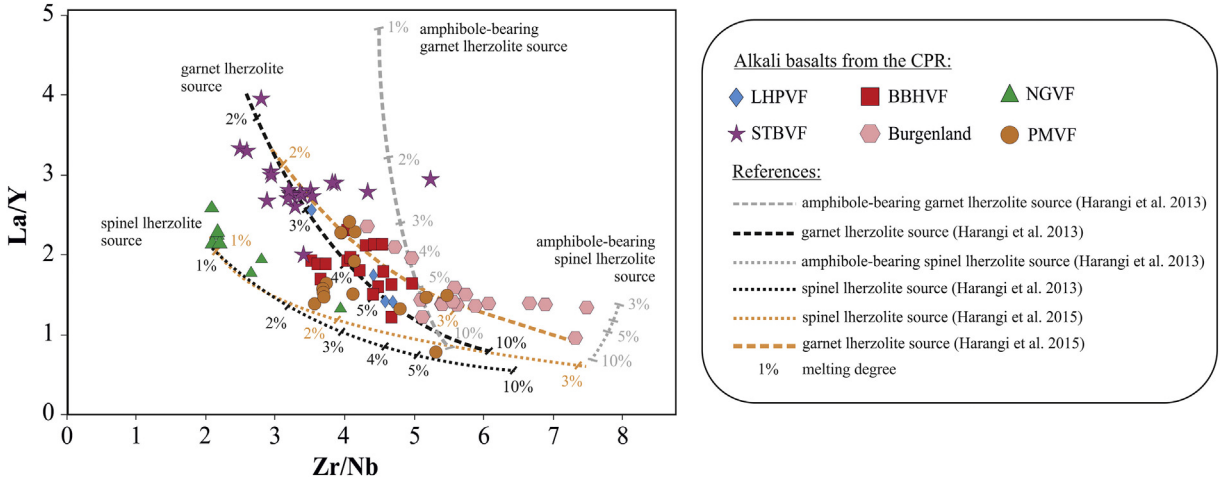

Fig. 4. Estimated degrees of partial melting in upper mantle source regions of alkaline basalts based on La/Y vs. Zr/Nb ratios, following two different methodologies explained in Harangi et al. (2013, 2015) for spinel- and garnet lherzolite assemblages with and without the presence of amphibole. Modelled melting trajectories and degrees are from Harangi et al. (2013, 2015). Data for different alkaline basaltic occurrences are from the following references: Burgenland: Embey-Isztin et al. (1993); Ali and Ntaflos (2011); SBVF: Embey-Isztin et al. (1993); Seghedi et al. (2004); Ali et al. (2013); BBHVF and LHPVF: Embey-Isztin et al. (1993); Harangi et al. (2015); NGVF: Embey-Isztin et al. (1993); Dobosi and Jenner (1999); Harangi et al. (2015); PMVF: Embey-Isztin et al. (1993); Downes et al. (1995); Harangi et al. (2013).

beneath the CPR (Hetényi et al., 2009), where migrated receiver function profiles suggest an accumulation of formerly subducted slabs.

It is generally accepted that subducted slabs can transport significant amounts of volatiles (especially 'water') back to the deep upper mantle (e.g. Fumagalli and Klemme, 2015). There is also a growing number of observations that this 'water' can be accumulated between major geophysical discontinuities at depths of 410 and 660 km in 'water'-rich minerals such as K-hollandite, wadsleyite and ringwoodite, which can have up to a few wt.% 'water' incorporated in their mineral structure (Mazza et al., 2019; Pearson et al., 2014). Recent studies introduced the concept of 'hydrous plumes' which originate from the top of this 'wet' transition zone and rise to the bottom of the lithosphere causing extension and magmatism but without thermal anomalies (Chen et al., 2015, 2017; Freitas et al., 2017; Kuritani et al., 2019; Liu et al., 2016; Wang et al., 2015). The negative buoyancy of 'hydrous plumes' comes from their elevated melt and volatile content provided by the presumably global 'melt layer' at the 410 km boundary (Freitas et al., 2017). The existence of such 'hydrous' plume underneath the CPR cannot be ruled out since the Penninic subducted slab reached this transition zone in the Cretaceous, while the Vardar slab reached it in the Paleogene (Hetényi et al., 2009). Thus, there was still a time interval of several tens of myr for 'this' hydrous plume to rise from the ~410 km discontinuity to the bottom of the lithosphere at ~100–120 km (e.g. Falus et al., 2000). This provides a rationale for further exploration of the potential role of 'hydrous plumes' in the geodynamical and geochemical evolution of the CPR (see Koptev et al., 2017). Note, however, that Cenozoic alkaline basalts in the CPR are characterised by OIB-like trace element patterns (e.g. Harangi et al., 2015; Seghedi et al., 2004) and positive Nb and Ta anomalies in the central part of the area. This implies that the 'water' in the source region is not directly liberated from subducted slabs. Instead, it is likely an inherited enriched mantle component originating from slab derived fluid and mantle wedge interaction and subsequent redistribution/recycling in the upper mantle (i.e., Bali et al., 2007; Berkesi et al., 2012). In addition, the Sr and Pb isotopic systematics indicates the presence of ancient enriched components in some alkaline basalts. This highlights the possibility that at least a portion of the 'water' in the source region may have had an even older component in the mantle than the one resulting from Mesozoic subduction.

In summary, prior subduction of the Penninic, Magura and Vardar Oceans beneath the CPR may have played an important role in hydrating the overlying mantle wedge (including the asthenosphere). The younger 'hydrous plumes' rising from the 'subduction graveyard' of these earlier oceanic slabs could also have a role in hydrating the upper mantle.

4.3. Effect of high 'water' content on the melting properties of the upper mantle

It appears crucial to evaluate whether the estimated 'water' concentration is sufficient to trigger partial melting in the asthenospheric source beneath the BBHVF. In Fig. 5, different empirically and theoretically determined solidi for peridotitic upper mantle (Green, 2015; Green et al., 2010, 2014; Katz et al., 2003; Kovács et al., 2012a, 2017) are highlighted along with a depth-temperature curve representative for the BBHVF (Kovács et al., 2017). Harangi et al. (2015) estimated that the partial melting under the BBHVF took place at depths between ~70 and 100 km (~2.2–2.9 GPa). In Fig. 5, the shaded region shows the estimated range of 'water' concentrations in the source region following the concentration outlines in the melting model of Katz et al. (2003).

The three different solidi were determined experimentally by Green et al. (2010, 2014), Green (2015) and Kovács et al. (2012a). The '*water saturated solidus*' (Fig. 5) highlights the temperature at which the upper mantle begins to melt when the bulk 'water' concentration exceeds ~0.4 wt.% and ~200 ppm 'water' above and below ~100 km, respectively. The '*water saturated solidus*' is at ~1000 °C between 70 and 100 km, which is significantly exceeded by the temperature (~1100–1250 °C) in this depth range based on the area specific geotherm (Fig. 5). This implies that the upper mantle would be in a partially molten state if there was more than ~0.4 wt. % 'water' in the bulk rock at depths above ~100 km. Since our estimations give 'only' 290–660 ppm 'water' in the source, this means that the *'water saturated solidus'* cannot explain the presence of partial melt in the asthenosphere. The *'dry solidus'* (Fig. 5), for which the bulk 'water' is less than 200 ppm, cannot explain the presence of partial melt at this depth either, because the temperature beneath the BBHVF remains considerably below that of the *'dry solidus'* (i.e. ~1300–1400 °C). The *'pargasite dehydration solidus'* (Fig. 5), which is the solidus if bulk 'water' concentration is between ~200 ppm and 0.4 wt.%, is at 1050–1100 °C between 70 and 100 km depth. The *'pargasite dehydration solidus'* temperature is higher for geochemically more fertile and lower for more refractory upper mantle (Niida and Green, 1999). This is because Na-rich amphibole in more fertile upper mantle is stable to higher temperatures. Because the composition of the upper mantle is at least moderately refractory beneath the BBHVF, the *'pargasite dehydration solidus'* should be closer to ~1050 °C (e.g Dobosi et al., 2010; Embey-Isztin et al., 2014; Kovács

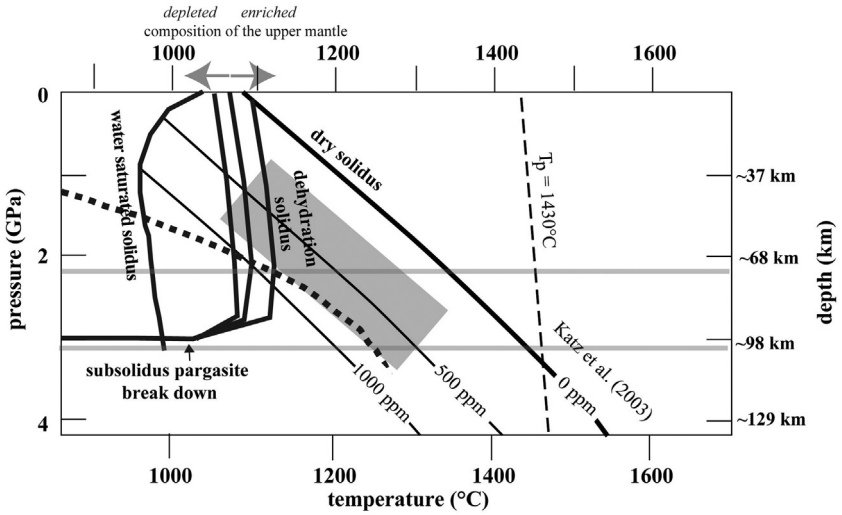

Fig. 5. Effect of water on solidus temperature of the upper mantle. The figure is modified and completed after Green (2015) and Kovács et al. (2017). Various solidi are indicated by solid black lines. The *i) water saturated solidus* is valid if the bulk water content in the upper mantle is >0.4 wt.%; The *ii) (pargasite) dehydration solidi* are the solidi when the bulk water content is between ~0.02 wt.% (~200 ppm) and 0.4 wt.% (~400 ppm) at depths shallower than ~100 km. Temperatures of the *pargasite dehydration solidi* are higher for more fertile and lower for more refractory compositions of the upper mantle. The solidus is the *iii) dry solidus* when the bulk water content is below ~0.02 wt.% (200 ppm). Calculated solidi positions from Katz et al. (2003) are also highlighted. Note that this calculation only includes the effect of hydrogen stored in nominally anhydrous minerals but does not incorporate the impact of hydrous minerals and excess fluid. Calculated solidi curves are determined for 500, 1000 and 3000 ppm water in the bulk rock. Pressure was converted to depth assuming lithostatic pressure only, with a 30 km thick crust (Bielik et al., 2018; Wéber, 2002) and crustal and upper mantle densities set at 2700 and 3300 kg/m^3 respectively. The geotherm is marked by a dashed bold black line and corresponds to 100 mW/m^2 surface heat flow typical for the central part of the Pannonian Basin as taken from Kovács et al. (2017). The grey shaded area indicates the minimum range of bulk water contents (~260–660 ppm wt. including 40% uncertainty and assuming 20% fractionation) in the source region of the studied alkaline basalts superimposed on the solidi positions calculated by Katz et al. (2003). Horizontal light grey lines indicate the pressure/depth range (between ~70 and ~90 km) of partial melting determined for the BBHVF basalts by Harangi et al. (2015).

et al., 2012a; Szabó et al., 2004). The geotherm exceeds the *'pargasite dehydration solidus'* in the entire depth range between 70 and 100 km from where alkaline basalts in the BBHVF originate (Fig. 5). Since the estimated range of 'water' concentrations in the source region almost perfectly overlaps with bulk 'water' contents where the solidus is the *'pargasite dehydration solidus'*, it is very likely that the asthenosphere must have been in a partially molten state at the time of alkaline basaltic volcanism. This means that the 'water' concentration alone would have been sufficient to trigger partial melting in the asthenosphere without the need for decompressional melting, thermal plumes or the direct effect of geochemical heterogeneities (i.e. eclogite or pyroxenite lithologies) in the mantle source.

The possible contribution of eclogite or pyroxenite lithologies to the basaltic melts was estimated following the experimentally developed methodology of Le Roux et al. (2011). These authors argue that the bulk concentration of a few major and trace elements (i.e., Fe, Mn, Co, Zn, Ni) in basalts and their particular ratios can distinguish effectively between peridotite, eclogite and mixed source lithologies based on their distinct partitioning into eclogites and peridotites (Fig. 6). In these diagrams, average whole-rock compositions of alkaline basalts from the CPR (including the BBHVF) are plotted. As the alkaline basalts may have gone through fractional crystallisation (see also our MELTS modelling above), we also plotted bulk assemblages to which both 10 and 20% of cumulates were added (i.e. Zajacz et al., 2007). This calculation serves the purpose of illustrating how the trace element compositions changed during fractional crystallization of alkaline basalts and how much contribution from eclogite and pyroxenite lithologies can be expected. The composition of cumulates was estimated by mixing 70 wt.% olivine (Type I olivine core from Jankovics et al., 2019) and 30 wt.% clinopyroxene (primitive colourless megacrysts from Jankovics et al., 2016). Both phases represent near liquidus minerals crystallising from almost unfractionated basaltic melts. In Fig. 6a ((Mn/Fe)·100 vs. (Co/Fe)·100), the average compositions all fall in the eclogite range. However, the recalculated less fractionated bulk compositions in this calculation (assuming 20% fractionation) is on the mixing line between 60% eclogite and 5% spinel peridotite partial melt in 30 and 70% proportions respectively. In contrast, in Fig. 6b (Mn/Zn vs. Ni/Co) almost all but the original (uncorrected) basalt compositions reside in or are very close to the peridotite field. The less fractionated average basalt composition of the BBHVF is on the garnet peridotite melting curve corresponding to a higher degree of partial melting without any contribution from eclogite melts. If the original and 10% fractionation corrected compositions are taken into account, implying contributions of 30% and 60% partial melts originating from eclogite (degree of which partial melting is as high as ~80%) and spinel peridotite (with significantly lower degree of partial melting). Average compositions of other alkaline basaltic fields from the CPR show similar patterns apart from moving towards either the spinel or garnet peridotite melting curves from that of eclogite. In Fig. 6c ((Mn/Fe)·100 vs. (Zn/Fe)·100), all basalts from the CPR are in the peridotite field. Both the original and fractionation corrected compositions fall in the continuation of the garnet peridotite melting trend. In summary, there is only one diagram where the 20% fractionation corrected composition from the BBHVF is in the eclogite field (Fig. 6a), but it indicates only 30% contribution of eclogite derived melts. In the other two scenarios (Fig. 6a and 5b) the same 20% fractionation corrected compositions of basalts from the BBHVF reside on the pure garnet peridotite melting curve. Even in case a lower degree of fractionation occurred, the contribution of eclogite melt remains below 30%. If, as indicated by the MELTS modelling, a higher degree of fractionation occurs (up to 40%), the trends move more towards the peridotite field indicating a reduced contribution from eclogite and pyroxenite lithologies. The diagrams point to a minor direct contribution of eclogite or pyroxenite derived melts to the basalts, which is also confirmed by the presence of subducted slab derived melts beneath the BBHVF (Bali et al., 2008). In contrast, garnet peridotite derived melts predominate in agreement with other geochemical trace element modelling (see Fig. 4). It follows that the role of eclogite lithologies in decreasing the solidus temperature of the upper mantle may have been only subordinate to that of 'water'.

From the above, it appears that the asthenosphere was sufficiently 'wet' to contain partial melt at the time of alkaline basaltic volcanism, and presumably also prior to this stage. Note that changing bulk

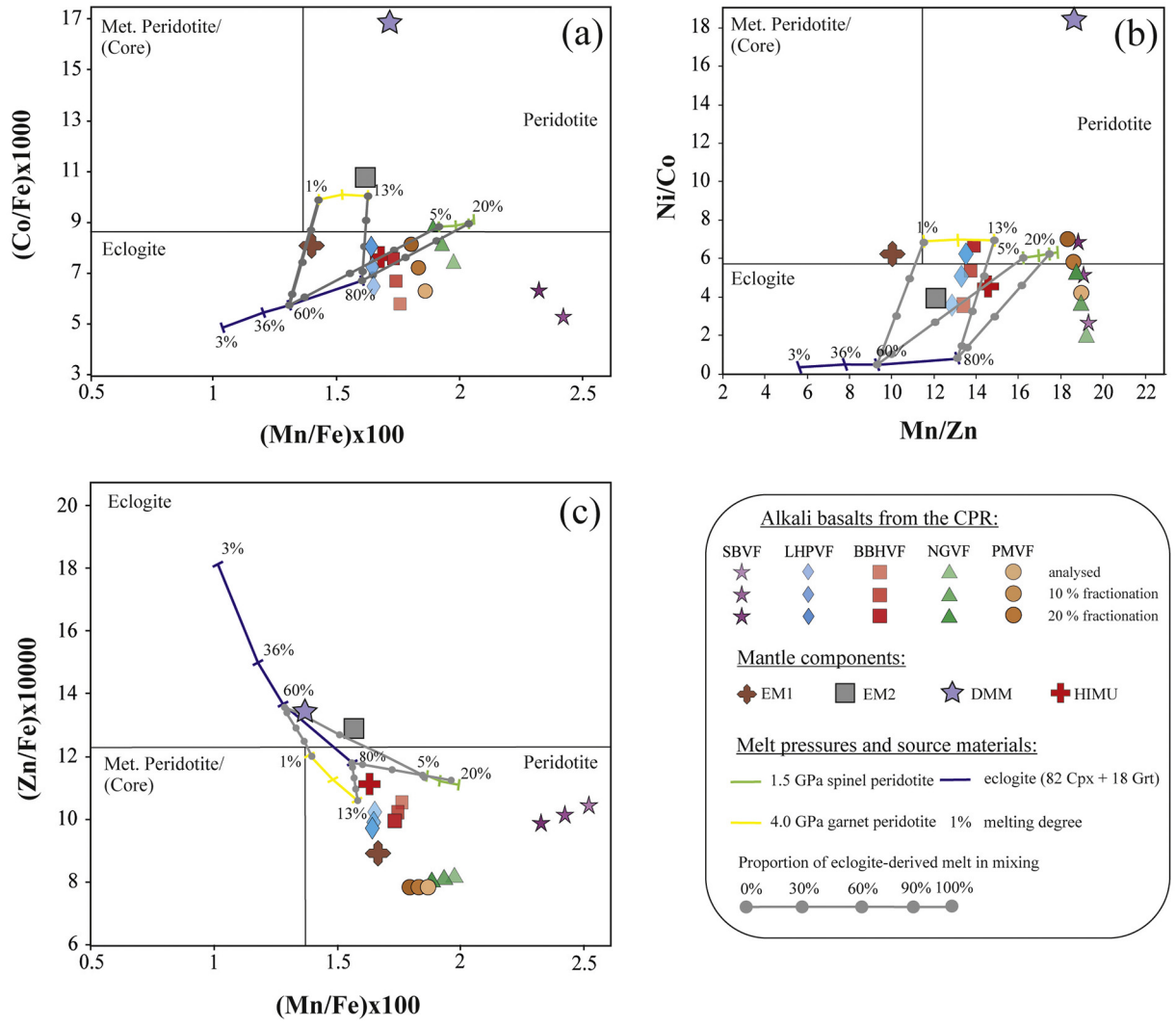

Fig. 6. Discrimination diagrams for Zn/Fe×10^4 vs Mn/Fe×100 (a), Ni/Co vs Mn/Zn (b) and Co/Fe vs Mn/Fe×100 (c) based on Le Roux et al. (2011). Average compositions for different alkaline basaltic volcanic fields were calculated based on the references listed in Fig. 4. Measured basalt compositions were corrected for fractional crystallization assuming 10 and 20% fractionation of a cumulate consisting of 70 wt.% olivine and 30 wt.% clinopyroxene. Compositions of olivine and clinopyroxene used in the model are averages of Type I olivine cores from Jankovics et al. (2019) and primitive colourless megacryst from Jankovics et al. (2016), respectively.

geochemistry of the upper mantle with special respect to other volatiles (i.e. CO_2, Cl^-, F^- and N_2) can slightly influence the temperature of the different solidi as well. The effect of the changing bulk geochemistry of the upper mantle (i.e. more refractory or more fertile) has been already addressed by experimental studies (e.g. Green, 2015) and seems to only subordinately modify the solidus temperature (±~50 °C) at a given pressure. The most important volatile component besides 'water' is CO_2 (e.g. Berkesi et al., 2012) with an effect indirectly taken into account since a trace amount of CO_2 is always present during experiments.

It is important to emphasise the novelty of our approach, based on the effect of a small amount of 'water' on the solidus. Some of the earlier experimental studies on the melting properties of the upper mantle (e.g. Grove et al., 2006; Mysen and Boettcher, 1975) simply omitted the role played by trace amounts of 'water' and hydrous phases, most importantly, pargasitic amphibole. It has been demonstrated only relatively recently (Green et al., 2010), that pargasitic amphibole is a stable phase of the upper mantle even from as low as ~200 ppm bulk 'water' contents up to ~0.4 wt.% at depths shallower than 100 km. Under these conditions the solidus is the *'pargasite dehydration solidus'* at ~ 1050–1100 °C; approximately 100–150 °C lower than without considering the effect of trace amount of 'water' and the stability of pargasitic amphibole.

Other experimental and theoretical studies (e.g. Hirschmann et al., 2009; Katz et al., 2003), however, simply assumed that the *'(nominally anhydrous) NAMs solidus'* temperature changes continuously with the concentration of structural hydroxyl in NAMs between the *'water saturated'* and *'dry'* solidi (see Fig. 5). Katz et al. (2003) proposed that the position of the *'NAMs solidus'* shifts to lower temperatures in the P-T space more or less parallel to the *'dry solidus'* (Fig. 5). According to this model at a given pressure (depth), 500 ppm 'water' incorporated as structural hydroxyl in NAMs lowers the solidus temperature by 100–150 °C with respect to the *'dry solidus'* (Fig. 5). The geotherm beneath the BBHVF would even intersect this *'NAMs solidus'* for higher (600–800 ppm) bulk 'water' contents which are still in the upper range of our estimates. Thus, even these theoretical models would predict the presence of partial melt in the upper mantle beneath the BBHVF.

At this stage there is still some uncertainty whether our results only concern the BBHVF or they could equally be relevant for other alkaline basaltic localities in the CPR. Since the BBHVF is one of the most distant alkaline basaltic sites – in its present position – from the suture zones of prior subductions (i.e. Penninic, Vardar and Magura) it is reasonable to assume that beneath other localities closer to these former subduction zones the degree of hydration may have been even more pronounced. Consequently, the asthenosphere should have been in partially molten

state under all alkaline basaltic localities of the CPR prior to and during the alkaline basaltic volcanic activity.

Therefore, it may not be the main question anymore why partial melting occurred in the asthenosphere beneath the BBHVF, but instead why the partial melt was extracted only in the tectonic inversion stage of the CPR?

4.4. What could drive melt extraction from the asthenosphere during the tectonic inversion and how?

If partial melt was present in the 'wet' asthenosphere beneath the central CPR, then the question arises what was unique in the tectonic inversion stage which facilitated its extraction from the asthenosphere and led to the formation of alkaline basaltic volcanoes on the surface. To address this issue, we first have to resolve which geodynamic processes characterised the tectonic inversion stage. The first regional tectonic process preceding the tectonic inversion stage was the 'docking' or 'soft collision' of the two major tectonic units (Alcapa and Tisza-Dacia) with the European platform in the Carpathian embayment at ~11 Ma (e.g. Csontos et al., 1992; Matenco et al., 2003). After this major tectonic event, the stress field did not change immediately to compression in the lithosphere since smaller scale block rotations, slip along major tectonic lines and nappe stacking could have taken up the shortening for a while. The tectonic inversion began at 8 and 5 Ma in the SW and E part of the Pannonian Basin, respectively (e.g. Bada et al., 2007; Balázs et al., 2016; Horváth and Cloetingh, 1996). The tectonic inversion and the accompanying shortening and compression were driven by the counter-clockwise rotation of the Adriatic indenter and its convergence to the stable European platform (e.g. Bada et al., 2007; Bus et al., 2009; Caporali, 2009). As a consequence, in the central part of the CPR, the compression is predominantly SW–NE directed since at least the onset of the inversion stage. Our main objective is to identify whether there are any geophysical and geological consequences of this compression in the lithosphere and asthenosphere which could facilitate the extraction of basaltic partial melts from the asthenosphere and their rise to the surface.

4.5. Deformation and stress regime in the asthenosphere and lithospheric mantle at the time of alkaline basaltic volcanic activity

A topic of prime importance concerns the role of the asthenosphere and the deeper lithospheric mantle. The direction of shear wave splitting (SKS) in the central part of the CPR is NW–SE directed which is perpendicular to the direction of main compression, with delay times around or less than 1 s (Fig. 7; Kovács et al., 2012b; Qorbani et al., 2016). An important question is how this information can be utilised to infer the deformation state of the asthenosphere and the lithospheric mantle. The splitting of seismic shear waves in the Earth's interior is due to anisotropy which originates from the lattice preferred orientation of rock forming minerals developing in response to stress. Consequently, olivine – the most deformable mineral of the asthenosphere (e.g. Tommasi et al., 1999; Vauchez et al., 2012) – usually develops lattice preferred orientations (LPO), for instance by its 'a' crystallographic axis turning into the foliation plane and parallel to the lineation. This is, however, not generally true since at different bulk 'water' contents and degrees of stress, various slip systems can also be active, resulting in different alignments of the major crystallographic axes with respect to the direction of the compression (Jung, 2009). The main point is that the less viscous asthenosphere (and also, to a smaller extent the lithospheric mantle) can develop LPO of minerals often generating macroscopic foliation and lineation in the upper mantle.

The degree of shear wave anisotropy can be constrained from the statistical analysis of electron backscatter diffraction (EBSD) determined LPO of the rock forming major silicate minerals and their physical properties (e.g. Mainprice et al., 2000). In the BBHVF, alkaline basalts brought up a significant amount of upper mantle xenoliths to the surface, providing an opportunity to determine the orientation and degree of their shear wave anisotropy (Falus, 2004). As geophysically determined SKS splitting delay time data are also available for the BBHVF (Kovács et al., 2012b; Qorbani et al., 2016), the thickness of the anisotropic layer and the orientation of the xenoliths in this layer can be estimated. As the original orientation of peridotite xenoliths in the upper mantle is unknown, several scenarios should be explored for how the foliation and lineation of these upper mantle rocks are aligned with

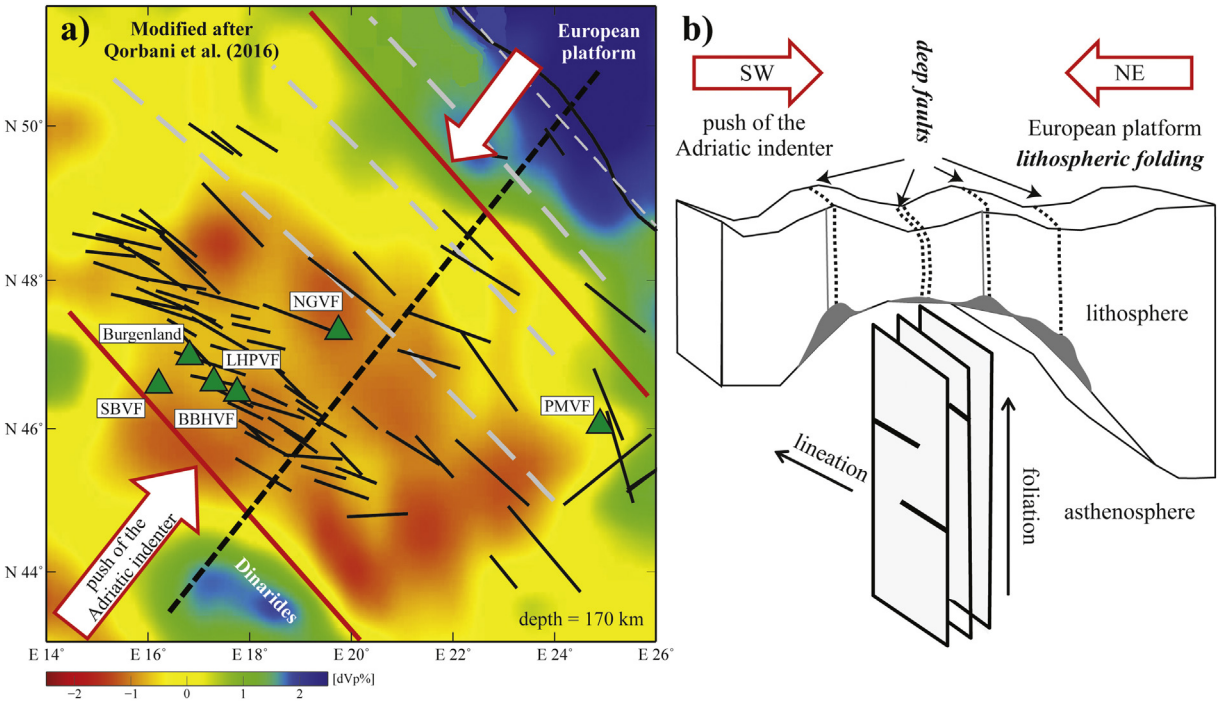

Fig. 7. Schematic map showing the direction of measured shear wave splitting in the region modified after Qorbani et al. (2016) (a), and a model explaining both the orientation of SKS splitting and the formation of alkaline basalts at the late-Neogene tectonic inversion stage of the Carpathian-Pannonian region (b).

respect to the almost vertically propagating seismic waves (e.g. Kovács et al., 2012b; Klébesz et al., 2015; Aradi et al., 2017; Liptai et al., 2018). As already demonstrated by Kovács et al. (2012b) for the BBHVF, we assume that the contribution of the crust and the lithospheric mantle to the observed SKS splitting was only moderate due to their smaller thickness and lower degree of anisotropy. Consequently, Kovács et al. (2012b) suggested a one layer model in which the degree of anisotropy is estimated by a representative xenolith typical for the deeper, more anisotropic part of the upper mantle beneath the BBHVF (which is thought to represent 'lithospherised' asthenosphere). From the examined scenarios, the one where the foliation plane is vertical and parallel to the direction of SKS splitting (NW–SE) and the lineation is horizontal (Fig. 7) provides the most realistic (i.e. smallest) anisotropic layer thickness for the BBHVF (~85 km, Kovács et al., 2012b). The thickness of the anisotropic layer matches the extent of thinning (~60–80 km) of the lithospheric mantle during extension when the asthenosphere rose from its pre-extensional depth of ~100–120 km (e.g. Falus et al., 2000; Huismans et al., 2001) to only ~40 km depth right at the end of the syn-rift stage (Kovács et al., 2012b). In addition, this depth difference also roughly coincides with the thickness of the asthenospheric dome trapped between the Adriatic indenter and the European platform (e.g. Tari et al., 1999; Tašárová et al., 2009). As the ambient thickness of the lithosphere outside of the Pannonian Basin is ~140–200 km whereas it is presently ~60 km in the central part of the basin (but the LAB was only at ~40 km depth after the extension), at least ~80 km asthenosphere was trapped between the converging main continental lithospheres.

Our interpretation is that the asthenospheric dome may have been under SW–NE compression between the very thick European platform (~200 km) and the Adriatic indenter (~140 km) at least since the termination of the syn-rift stage due to the northward movement and counterclockwise rotation of the Adrian promontory. This compression developed NW–SE directed, near vertical foliation and horizontal lineation in the upper mantle (Fig. 7). Compression induced deformation resulted in foliation planes becoming increasingly vertical, providing pathways for partial melts towards the surface. It is likely that the foliation plane prior to the end of the 'syn-rift' stage was closer to horizontal due to the dominant extensional tectonic regime. The extension exerted horizontal stretching in the lithosphere, which may have been also accompanied, and even driven by sub-horizontally directed flow in the underlying asthenosphere (e.g. Kovács et al., 2012b).

It is, therefore, likely that a near vertical foliation in the asthenosphere (and probably also in the lithospheric mantle to a smaller extent) under a compressional stress regime has facilitated the extraction of partial melts from the asthenosphere and channelised the accumulated melt towards the surface. An outstanding question is how partial melts could penetrate the crust and the lithospheric mantle.

4.6. Recent deep crustal deformation and stress regime

The whole lithosphere-asthenosphere system appears to be under NE–SW compression at least from the onset of the tectonic inversion stage (~8–5 Ma) but the asthenosphere may have been under compression since the main tectonic units were docked in the Carpathian embayment at ~11 Ma. Focal mechanisms of earthquakes and deep magnetic soundings provide information on the prevailing stress directions in the crust. Focal mechanisms of earthquakes from the Pannonian Basin with depths commonly up to ~10 km are mostly of strike-slip character with only a few characterised by thrust faulting. Especially in the central part of the Pannonian Basin (also close to the BBHVF), the compressional axes of the determined moment tensors are NE-SW oriented (Wéber, 2018). This means that the direction of the main compression in the shallower crust agrees well with that of the asthenosphere and deeper lithospheric mantle. The directions of geomagnetic induction vectors in the well conducting zones of the BBHVF are also mostly SW–NE oriented (Ádám et al., 2017; Ádám and Wesztergom, 2001). This direction implies the existence of NW–SE directed deep conducting fractures in the area. Borehole breakout data, especially in the southern part of the Great Hungarian Plain in the very shallow crust (up to a few kilometers), also provide evidence for a mainly NE–SW orientation of the compressional stress field (Bada et al., 2007).

It is therefore evident, that the compression and its direction in the asthenosphere and deep lithospheric mantle at the time of the alkaline basaltic volcanic activity is strikingly similar to the present-day stress field in the crust revealed by focal mechanism solutions of earthquakes and geomagnetic induction vectors. This NE–SW direction of the compression is parallel with the convergence between the Adriatic indenter and the stable European platform indicated by NE oriented movements of major tectonic units in most parts of the Pannonian Basin (Caporali, 2009; Grenerczy et al., 2005).

4.7. Lithospheric-scale folding

The asthenosphere and the lithosphere have responded differently to the compression due to their contrasting rheological properties. The asthenosphere is rheologically much weaker and takes up the compression dominantly by ductile deformation which probably adjusts the LPO of minerals to the dominating stress field relatively quickly on geological time scales. In contrast, the upper crust is rheologically much stronger and deforms usually in a brittle way, thus taking much longer to readjust its fabric to the prevailing stress directions (i.e., it has a longer memory of prior stress regimes). We propose that while the asthenosphere developed near vertical foliation and horizontal lineation as a response to the compressional stress field, the lithosphere was folded (Cloetingh et al., 1999, 2003; Dombrádi et al., 2010). Lithospheric-scale folding may have generated deep fractures cutting through the entire lithosphere, particularly along the axes of long wavelength (few hundred km) anticlines and synclines where deformation is most intense (Fig. 7). The focal mechanism solutions of earthquakes and geomagnetic induction vectors all indicate the presence of NW–SE directed fractures or deformation zones which are thought to be parallel to the strike of these supposed anticlines and synclines of the folded lithosphere. Thus, it seems logical to assume that lithospheric scale folding and the associated formation of deep 'fractures' or deformation zones in the lithosphere provide pathways for basaltic partial melts squeezed from the asthenosphere to rise all the way to the surface (Fig. 7). In summary, the NW–SE directed foliation in the asthenosphere and 'fractures' or deformation zones in the lithosphere developed due to the NE–SW compression during the tectonic inversion stage of the CPR and facilitated the extraction and channelling of partial melts from the 'wet' asthenosphere to the surface. Previous volcanological studies also argued that the alkaline basaltic activity was mainly tectonically controlled because both the magma flux and output rate were low (Kereszturi et al., 2010). Martin and Németh (2004) also proposed that the tectonic inversion in the CPR might have played a role in the formation of alkaline basalts of the BBHVF as well.

This process is likely not only of local importance, but could have general relevance as it provides an explanation for the formation of (alkaline) basalts in extensional basins subject to late-stage compression. In addition, it also sheds light on the occurrence of alkaline basaltic volcanism in transpressional tectonic regimes where the asthenospheric source is 'wet'.

4.8. Spatial aspects of the Plio-Pleistocene alkaline basaltic volcanic activity in the CPR

A closer look at the spread of alkaline basalt outcrops within the main alkaline basaltic localities in the CPR can yield a somewhat blurred image. At each volcanic field, the volcanic formations follow a more or less systematic pattern. In the Styrian basin (SBVF) the volcanic formations appear to align along two major directions: a major NW–SE and a subordinate SW–NE direction perpendicular to the former (Bojar et al.,

2013). In the Nógrád-Gömör (NGVF) volcanic field the main alkaline-basaltic volcanic formations can be found along the NW-SE direction from Maskófalva (Maškova) to Bárna although a second, perpendicular alignment is not as characteristic as seen in the SBVF (e.g. Hovorka and Fejdi, 1980; Szabó and Taylor, 1994). In the LHPVF and BBHVF, at first sight there are no clear and obvious directions as in the previous cases (i.e. SBVF and NGVF). The NW-SE direction, however, can be recognized in the Ság Mt.–Somló–Kab Mt.–Tihany line outlined by alkaline basaltic formations on the surface (e.g. Szabó et al., 2010). To a smaller extent, this direction can also be detected from magnetic anomalies presumably corresponding to subsurface basaltic formations and from surface outcrops of basalts aligned roughly along the Uzsa–Badacsony–Fonyód line. In addition, a NE-SW direction is also present stretching roughly from Balatonszentgyörgy to the Kab Mt. From surface outcrops and geomagnetic surveys it appears that NW-SE and SW-NE directions are also present in the LHPVF and BBHVF volcanic fields (Kiss et al., 2017; Visnovitz et al., 2018)

Overall, it seems that for the majority of the alkaline basaltic volcanic fields, a NW–SE direction is the dominant orientation along which alkaline basaltic volcanic formations are aligned. Subordinately a perpendicular SW–NE direction is present as well, which is similar to the strike of major tectonic lines (i.e. Balaton Line, Kapos line; Fodor et al., 1999). Furthermore, in a broader perspective of the CPR, the smaller volcanic formations at Kecel (Danube-Tisza interfluve), Lucareţ (Banat region), and Štiavnica basalts (Central Slovakian volcanic field) may also be aligned along this main, NW–SE direction (Fig. 1). Thus alkaline basalts erupted along zones mainly perpendicular to the present day NE-SW compression or subordinately parallel to it.

4.9. Possible salt diapir analogy for the partially molten asthenosphere in compressional settings

Modelling studies of salt tectonics have demonstrated that salt layers overlain by rheologically stronger and more viscous formations can be effectively mobilised by horizontal compression (e.g. Stephenson et al., 1992; Daudré and Cloetingh, 1994). During this process, salt starts to rise along localised, narrow vertical wall-like zones. In contrast, during extension, similar geometries develop with a much smaller extent of vertical movements. We hypothesise that the low viscosity asthenospheric dome under a more rigid extended lithospheric lid may respond to compression in a mode similar to salt domes. Thus, the asthenosphere may rise along narrow (few to a few tens of kilometres) and deep sub-vertical zones of the deforming lithosphere causing local heat flow, geophysical anomalies and possibly triggering localised volcanic activity. Thus it may well be that there is no strict need for assuming the existence of 'plume fingers' to explain the presence of small scale regional geophysical and geochemical anomalies in the lithosphere as rising asthenosphere – analogous to salt under compression – along narrow deformation zones (Fig. 7b) of the lithosphere may equally well explain these observations.

5. Conclusions

The asthenosphere was 'wet' (290–660 ppm 'water' content) at the time of alkaline basaltic volcanism in the Carpathian-Pannonian-region (CPR) and with such bulk 'water' contents the asthenosphere was above the *'pargasite dehydration solidus'*. The 'wet' character of the asthenosphere below the CPR may have been due to the hydration of the mantle wedge above the former Penninic, Vardar and Magura subducting slabs and/or 'hydrous' plumes originating from the 'subduction graveyard' under the region. Thermal plumes and eclogite and pyroxenite lithologies did play at most a minor role in the formation of partial melts in the asthenosphere.

The partial melts in the asthenosphere were extracted and channelled to the surface during the tectonic inversion stage under a compressional tectonic regime. The tectonic inversion generated compression in the lithosphere and asthenosphere which resulted in foliation and lineation in the asthenosphere and folding of the lithosphere. In combination with compression, near vertical foliation in the asthenosphere facilitated extraction and channelling of partial melts from the asthenosphere towards the surface. Simultaneously, folding of the lithosphere may have led to the formation of deep fractures and deformation zones crosscutting the entire lithosphere most probably in the axes of anticlines and synclines of the folding. These deep zones were important in providing further pathways for basaltic melts extracted from the asthenosphere towards the surface.

This implies that if the asthenosphere is 'wet' (>>200 ppm) and temperature exceeds the *'pargasite dehydration'* and *'water saturated'* solidi (both in the range of 1000–1100 °C) above and below 100 km, respectively, basaltic partial melt can be present and transported to the surface even in a compressional stress regime. This model may provide a conceptual framework for continental extensional (back-arc) basins undergoing late-stage compression and for continental transpressional zones in the lithosphere in general.

Declaration of Competing Interests

The authors declare that they have no known competing financial interests or personal relationships that could have appeared to influence the work reported in this paper.

Acknowledgements

The authors acknowledge the support of the MTA CSFK Lendület Pannon LithH_2Oscope grant, and the NKFIH K128122 grant. Constructive discussions on geochemistry, volcanology, geochronology, space geodesy and magnetotellurics with Alexandru Szakács, Zoltán Pécskay, Marinel Kovacs, Antal Ádám, Szabolcs Harangi, Péter Luffi, Qunke Xia, Huan Chen, Liu Jia and Eszter Szűcs helped us to further develop our concepts. We are grateful to the managing Editor (Costanza Bonadiman) and two anonymous reviewers for constructive reviews and comments. K. Hidas acknowledges funding by the "Agencia Estatal de Investigation" (AEI, Spain) project no. CGL2016-81085-R. L.E. Aradi's, Gy. Falus's and Cs. Szabó's work was funded by the Eötvös Loránd University (ELTE) Institutional Excellence Program (1783-3/2018/FEKUTSRAT) supported by the Hungarian Ministry of Human Capacities. S.A.P.L. Cloetingh was supported by the Distinguished Guest Scientist Fellowship Program of the Hungarian Academy of Sciences. L. Patkó was supported by the GINOP-2.3.2-15-2016-00009 research program.

References

Ádám, A., Wesztergom, V., 2001. An attempt to map the depth of the electrical asthenosphere by deep magnetotelluric measurements in the Pannonian Basin (Hungary). Acta Geol. Hung. 44 (2-3), 167–192.

Ádám, A., Szarka, L., Novák, A., Wesztergom, V., 2017. Key results on deep electrical conductivity anomalies in the Pannonian Basin (PB), and their geodynamic aspects. Acta Geod. Geophys. 52 (2), 205–228.

Ali, S., Ntaflos, T., 2011. Alkali basalts from Burgenland, Austria: Petrological constraints on the origin of the westernmost magmatism in the Carpathian–Pannonian Region. Lithos 121 (1-4), 176–188.

Ali, S., Ntaflos, T., Upton, B.G., 2013. Petrogenesis and mantle source characteristics of Quaternary alkaline mafic lavas in the western Carpathian–Pannonian Region, Styria, Austria. Chem. Geol. 337, 99–113.

Aradi, L.E., Hidas, K., Kovács, I.J., Tommasi, A., Klébesz, R., Garrido, C.J., Szabó, C., 2017. Fluid-enhanced annealing in the subcontinental lithospheric mantle beneath the westernmost margin of the Carpathian-Pannonian extensional basin system. Tectonics 36 (12), 2987–3011.

Arcay, D., Tric, E., Doin, M.P., 2005. Numerical simulations of subduction zones: Effect of slab dehydration on the mantle wedge dynamics. Phys. Earth Planet. In. 149 (1-2), 133–153.

Arcay, D., Doin, M.P., Tric, E., Bousquet, R., de Capitani, C., 2006. Overriding plate thinning in subduction zones: Localized convection induced by slab dehydration. Geochem. Geophys. Geosyst. 7 (2).

Asimow, P.D., Dixon, J.E., Langmuir, C.H., 2004. A hydrous melting and fractionation model for mid-ocean ridge basalts: Application to the Mid-Atlantic Ridge near the Azores. Geochem. Geophys. Geosyst. 5 (1).

Aubaud, C., Hauri, E.H., Hirschmann, M.M., 2004. Hydrogen partition coefficients between nominally anhydrous minerals and basaltic melts. Geophys. Res. Lett. 31 (20).

Bada, G., Horváth, F., Dövényi, P., Szafián, P., Windhoffer, G., Cloetingh, S., 2007. Present-day stress field and tectonic inversion in the Pannonian basin. Global Planet. Change 58 (1-4), 165–180.

Balázs, A., Matenco, L., Magyar, I., Horváth, F., Cloetingh, S.A.P.L., 2016. The link between tectonics and sedimentation in back-arc basins: New genetic constraints from the analysis of the Pannonian Basin. Tectonics 35 (6), 1526–1559.

Bali, E., Falus, G., Szabó, C., Peate, D.W., Hidas, K., Török, K., Ntaflos, T., 2007. Remnants of boninitic melts in the upper mantle beneath the central Pannonian Basin? Mineral. Petrol. 90 (1-2), 51–72.

Bali, E., Zajacz, Z., Kovacs, I., Szabó, C.S., Halter, W., Vaselli, O., Török, K., Bodnar, R.J., 2008. A quartz-bearing orthopyroxene-rich websterite xenolith from the Pannonian Basin, Western Hungary: evidence for release of quartz-saturated melts from a subducted slab. J. Petrol. 49 (3), 421–439.

Balogh, K., Mihalikova, A., Vass, D., 1981. Radiometric dating of basalts in southern and central Slovakia. Zapadne Karpaty, Seria Geologia, pp. 113–126.

Berkesi, M., Guzmics, T., Szabó, C., Dubessy, J., Bodnar, R.J., Hidas, K., Ratter, K., 2012. The role of CO_2-rich fluids in trace element transport and metasomatism in the lithospheric mantle beneath the Central Pannonian Basin, Hungary, based on fluid inclusions in mantle xenoliths. Earth Planet. Sci. Lett. 331, 8–20.

Berkesi, M., Czuppon, G., Szabó, C., Kovács, I., Ferrero, S., Boiron, M.C., Peiffert, C., 2019. Pargasite in fluid inclusions of mantle xenoliths from northeast Australia (Mt. Quincan): Evidence of interaction with asthenospheric fluid. Chem. Geol. 508, 182–196.

Bielik, M., Makarenko, I., Csicsay, K., Legostaeva, O., Starostenko, V., Savchenko, A., Šimonová, B., Dérerová, J., Fojtíková, L., Pašteka, R., Vozár, J., 2018. The refined Moho depth map in the Carpathian-Pannonian region. Contrib. Geophys. Geod. 48 (2), 179–190.

Bojar, H.P., Bojar, A.V., Hałas, S., Wójtowicz, A., 2013. K/Ar geochronology of igneous amphibole phenocrysts in Miocene to Pliocene volcaniclastics, Styrian Basin, Austria. Geol. Quart. 57 (3), 405–416.

Bonadiman, C., Hao, Y., Coltorti, M., Dallai, L., Faccini, B., Huang, Y., Xia, Q., 2009. Water contents of pyroxenes in intraplate lithospheric mantle. Eur. J. Mineral. 21 (3), 637–647.

Bus, Z., Grenerczy, G., Tóth, L., Mónus, P., 2009. Active crustal deformation in two seismogenic zones of the Pannonian region—GPS versus seismological observations. Tectonophysics 474 (1-2), 343–352.

Caporali, A., 2009. Lithospheric flexure, uplift and expected horizontal strain rate in the Pannonian Carpathian region. Tectonophysics 474 (1-2), 337–342.

Chen, H., Xia, Q.K., Ingrin, J., Jia, Z.B., Feng, M., 2015. Changing recycled oceanic components in the mantle source of the Shuangliao Cenozoic basalts, NE China: New constraints from water content. Tectonophysics 650, 113–123.

Chen, H., Xia, Q.K., Ingrin, J., Deloule, E., 2017. Heterogeneous source components of intraplate basalts from NE China induced by the ongoing Pacific slab subduction. Earth Planet. Sci. Lett. 459, 208–220.

Chernyshev, I.V., Konečný, V., Lexa, J., Kovalenker, V.A., Jeleň, S., Lebedev, V.A., Goltsman, Y.V., 2013. K-Ar and Rb-Sr geochronology and evolution of the Štiavnica stratovolcano (Central Slovakia). Geol. Carpath. 64 (4), 327–360.

Cloetingh, S.A.P.L., Burov, E., Poliakov, A., 1999. Lithosphere folding: Primary response to compression? (from central Asia to Paris basin). Tectonics 18 (6), 1064–1083.

Cloetingh, S.A.P.L., Horváth, F., Dinu, C., Stephenson, R.A., Bertotti, G., Bada, G., Matenco, L., Garcia-Castellanos, D., TECTOP Working Group, 2003. Probing tectonic topography in the aftermath of continental convergence in central Europe. Eos, Trans. Am. Geophys. Union 84 (10), 89–93.

Csontos, L., Vörös, A., 2004. Mesozoic plate tectonic reconstruction of the Carpathian region. Palaeogeogr. Palaeoclimatol. Palaeoecol. 210 (1), 1–56.

Csontos, L., Nagymarosy, A., Horváth, F., Kovac, M., 1992. Tertiary evolution of the Intra-Carpathian area: A model. Tectonophysics 208 (1-3), 221–241.

Dando, B.D.E., Stuart, G.W., Houseman, G.A., Hegedüs, E., Brückl, E., Radovanović, S., 2011. Teleseismic tomography of the mantle in the Carpathian-Pannonian region of central Europe. Geophys. J. Int. 186 (1), 11–31.

Daudré, B., Cloetingh, S.A.P.L., 1994. Numerical modelling of salt diapirism: Influence of the tectonic regime. Tectonophysics 240 (1-4), 59–79.

Demouchy, S., Bolfan-Casanova, N., 2016. Distribution and transport of hydrogen in the lithospheric mantle: A review. Lithos 240, 402–425.

Demouchy, S., Jacobsen, S.D., Gaillard, F., Stern, C.R., 2006. Rapid magma ascent recorded by water diffusion profiles in mantle olivine. Geology 34 (6), 429–432.

Denis, C.M., Alard, O., Demouchy, S., 2015. Water content and hydrogen behaviour during metasomatism in the uppermost mantle beneath Ray Pic volcano (Massif Central, France). Lithos 236, 256–274.

Dixon, J.E., Stolper, E., Delaney, J.R., 1988. Infrared spectroscopic measurements of CO2 and H2O in Juan de Fuca Ridge basaltic glasses. Earth Planet. Sci. Lett. 90 (1), 87–104.

Dixon, J.E., Leist, L., Langmuir, C., Schilling, J.G., 2002. Recycled dehydrated lithosphere observed in plume-influenced mid-ocean-ridge basalt. Nature 420 (6914), 385–389.

Dixon, J.E., Dixon, T.H., Bell, D.R., Malservisi, R., 2004. Lateral variation in upper mantle viscosity: Role of water. Earth Planet. Sci. Lett. 222 (2), 451–467.

Dobosi, G., Jenner, G.A., 1999. Petrologic implications of trace element variation in clinopyroxene megacrysts from the Nograd volcanic province, north Hungary: A study by laser ablation microprobe-inductively coupled plasma-mass spectrometry. Lithos 46 (4), 731–749.

Dobosi, G., Jenner, G.A., Embey-Isztin, A., Downes, H., 2010. Cryptic metasomatism in clino-and orthopyroxene in the upper mantle beneath the Pannonian region. Geol. Soc. Lond. Spec. Publ. 337 (1), 177–194.

Dombrádi, E., Sokoutis, D., Bada, G., Cloetingh, S., Horváth, F., 2010. Modelling recent deformation of the Pannonian lithosphere: lithospheric folding and tectonic topography. Tectonophysics 484 (1-4), 103–118.

Downes, H., Seghedi, I., Szakács, A., Dobosi, G., James, D.E., Vaselli, O., Rigby, I.J., Ingram, G.A., Rex, D., Pécskay, Z., 1995. Petrology and geochemistry of late Tertiary/Quaternary mafic alkaline volcanism in Romania. Lithos 35, 65–81.

Embey-Isztin, A., Downes, H., James, D.E., Upton, B.G.J., Dobosi, G., Ingram, G.A., Harmon, R.S., Scharbert, H.G., 1993. The petrogenesis of Pliocene alkaline volcanic rocks from the Pannonian Basin, Eastern Central Europe. J. Petrol. 34 (2), 317–343.

Embey-Isztin, A., Dobosi, G., Bodinier, J.L., Bosch, D., Jenner, G.A., Pourtales, S., Bruguier, O., 2014. Origin and significance of poikilitic and mosaic peridotite xenoliths in the western Pannonian Basin: geochemical and petrological evidences. Contrib. Mineral. Petrol. 168 (3), 1054.

Falus, G., 2004. Microstructural analysis of upper mantle peridotites: their application in understanding mantle processes during the formation of the Intra-Carpathian Basin System. [PhD thesis]. Lithosphere Fluid Research Lab, University of Szeged, p. 163.

Falus, G., Szabó, C., Vaselli, O., 2000. Mantle upwelling within the Pannonian Basin: evidence from xenolith lithology and mineral chemistry. Terra Nova 12 (6), 295–302.

Ferriss, E., Plank, T., Walker, D., 2016. Site-specific hydrogen diffusion rates during clinopyroxene dehydration. Contrib. Mineral. Petrol. 171 (6), 55.

Fodor, L., Csontos, L., Bada, G., Györfi, I., Benkovics, L., 1999. Tertiary tectonic evolution of the Pannonian Basin system and neighbouring orogens: A new synthesis of palaeostress data. Geol. Soc. Lond. Spec. Publ. 156 (1), 295–334.

Freitas, D., Manthilake, G., Schiavi, F., Chantel, J., Bolfan-Casanova, N., Bouhifd, M.A., Andrault, D., 2017. Experimental evidence supporting a global melt layer at the base of the Earth's upper mantle. Nat. Commun. 8 (1), 2186.

Fumagalli, P., Klemme, S., 2015. Mineralogy of the earth: Phase transitions and mineralogy of the upper mantle. (editor-in-chief). In: Schubert, Gerald (Ed.), Treatise on Geophysics, 2nd edition Vol 2. Elsevier, Oxford, pp. 7–31.

Gerya, T.V., Perchuk, L.L., Maresch, W.V., Willner, A.P., Reenen, D.D.V., Smit, C.A., 2002. Thermal regime and gravitational instability of multi-layered continental crust: Implications for the buoyant exhumation of high-grade metamorphic rocks. Eur. J. Mineral. 14 (4), 687–699.

Ghiorso, M.S., Gualda, G.A., 2015. An H 2 O–CO 2 mixed fluid saturation model compatible with rhyolite-MELTS. Contrib. Mineral. Petrol. 169 (6), 53.

Green, D.H., 2015. Experimental petrology of peridotites, including effects of water and carbon on melting in the Earth's upper mantle. Phys. Chem. Miner. 42 (2), 95–122.

Green, D.H., Falloon, T.J., 2005. Primary magmas at mid-ocean ridges," hotspots," and other intraplate settings: Constraints on mantle potential temperature. Sp. Pap. Geol. Soc. Am. 388, 217.

Green, D.H., Hibberson, W.O., Kovács, I., Rosenthal, A., 2010. Water and its influence on the lithosphere–asthenosphere boundary. Nature 467 (7314).

Green, D.H., Hibberson, W.O., Rosenthal, A., Kovács, I., Yaxley, G.M., Falloon, T.J., Brink, F., 2014. Experimental study of the influence of water on melting and phase assemblages in the upper mantle. J. Petrol. 55 (10), 2067–2096.

Grenerczy, G., Sella, G., Stein, S., Kenyeres, A., 2005. Tectonic implications of the GPS velocity field in the northern Adriatic region. Geophys. Res. Lett. 32 (16).

Grove, T.L., Chatterjee, N., Parman, S.W., Médard, E., 2006. The influence of H_2O on mantle wedge melting. Earth Planet. Sci. Lett. 249 (1-2), 74–89.

Gualda, G.A., Ghiorso, M.S., Lemons, R.V., Carley, T.L., 2012. Rhyolite-MELTS: A modified calibration of MELTS optimized for silica-rich, fluid-bearing magmatic systems. J. Petrol. 53 (5), 875–890.

Hao, Y., Xia, Q., Li, Q., Chen, H., Feng, M., 2014. Partial melting control of water contents in the Cenozoic lithospheric mantle of the Cathaysia block of South China. Chem. Geol. 380, 7–19.

Hao, Y.T., Xia, Q.K., Jia, Z.B., Zhao, Q.C., Li, P., Feng, M., Liu, S.C., 2016. Regional heterogeneity in the water content of the Cenozoic lithospheric mantle of Eastern China. J. Geophys. Res. Solid Earth 121 (2), 517–537.

Harangi, S., Lenkey, L., 2007. Genesis of the Neogene to Quaternary volcanism in the Carpathian-Pannonian region: Role of subduction, extension, and mantle plume. Sp. Pap. Geol. Soc. Am. 418, 67.

Harangi, S., Sági, T., Seghedi, I., Ntaflos, T., 2013. Origin of basaltic magmas of Perşani volcanic field, Romania: A combined whole rock and mineral scale investigation. Lithos 180, 43–57.

Harangi, S., Jankovics, M.É., Sági, T., Kiss, B., Lukács, R., Soós, I., 2015. Origin and geodynamic relationships of the Late Miocene to Quaternary alkaline basalt volcanism in the Pannonian basin, eastern–central Europe. Int. J. Earth Sci. 104 (8), 2007–2032.

Hetényi, G., Stuart, G.W., Houseman, G.A., Horváth, F., Hegedűs, E., Brückl, E., 2009. Anomalously deep mantle transition zone below Central Europe: evidence of lithospheric instability. Geophys. Res. Lett. 36 (21).

Hirschmann, M.M., Stolper, E.M., 1996. A possible role for garnet pyroxenite in the origin of the "garnet signature" in MORB. Contrib. Mineral. Petrol. 124 (2), 185–208.

Hirschmann, M.M., Tenner, T., Aubaud, C., Withers, A.C., 2009. Dehydration melting of nominally anhydrous mantle: The primacy of partitioning. Phys. Earth Planet. In. 176 (1-2), 54–68.

Horváth, F., 1993. Towards a mechanical model for the formation of the Pannonian basin. Tectonophysics 226 (1-4), 333–357.

Horváth, F., Cloetingh, S.A.P.L., 1996. Stress-induced late-stage subsidence anomalies in the Pannonian basin. Tectonophysics 266 (1-4), 287–300.

Horváth, F., Bada, G., Szafián, P., Tari, G., Ádám, A., Cloetingh, S., 2006. Formation and deformation of the Pannonian Basin: constraints from observational data. Geol. Soc. Lond. Mem. 32 (1), 191–206.

Horváth, F., Musitz, B., Balázs, A., Végh, A., Uhrin, A., Nádor, A., Koroknai, B., Pap, N., Tóth, T., Wórum, G., 2015. Evolution of the Pannonian basin and its geothermal resources. Geothermics 53, 328–352.

Hovorka, D., Fejdi, P., 1980. Spinel peridotite xenoliths in the west Carpathian late Cenozoic alkali basalts and their tectonic significance. Bull. Volcanol. 43 (1), 95.

Huismans, R.S., Podladchikov, Y.Y., Cloetingh, S., 2001. Dynamic modeling of the transition from passive to active rifting, application to the Pannonian basin. Tectonics 20 (6), 1021–1039.

Jankovics, M.É., Harangi, S., Kiss, B., Ntaflos, T., 2012. Open-system evolution of the Füzestó alkaline basaltic magma, western Pannonian Basin: Constraints from mineral textures and compositions. Lithos 140, 25–37.

Jankovics, M.É., Taracsák, Z., Dobosi, G., Embey-Isztin, A., Batki, A., Harangi, S., Hauzenberger, C.A., 2016. Clinopyroxene with diverse origins in alkaline basalts from the western Pannonian Basin: Implications from trace element characteristics. Lithos 262, 120–134.

Jankovics, M.É., Sági, T., Astbury, R.L., Petrelli, M., Kiss, B., Ubide, T., Németh, K., Ntaflos, T., Harangi, Sz, 2019. Olivine major and trace element compositions coupled with spinel chemistry to unravel the magmatic systems feeding monogenetic basaltic volcanoes. J. Volcanol. Geotherm. Res. 369, 203–223.

Jung, H., 2009. Deformation fabrics of olivine in Val Malenco peridotite found in Italy and implications for the seismic anisotropy in the upper mantle. Lithos 109 (3-4), 341–349.

Kang, P., Lamb, W.M., Drury, M., 2017. Using mineral equilibria to estimate H2O activities in peridotites from the Western Gneiss Region of Norway. Am. Mineral. 102 (5), 1021–1036.

Karamata, S., 2006. The geological development of the Balkan Peninsula related to the approach, collision and compression of Gondwanan and Eurasian units. Geol. Soc. Lond. Spec. Publ. 260 (1), 155–178.

Katz, R.F., Spiegelman, M., Langmuir, C.H., 2003. A new parameterization of hydrous mantle melting. Geochem. Geophys. Geosyst. 4 (9).

Kereszturi, G., Csillag, G., Németh, K., Sebe, K., Balogh, K., Jáger, V., 2010. Volcanic architecture, eruption mechanism and landform evolution of a Plio/Pleistocene intracontinental basaltic polycyclic monogenetic volcano from the Bakony-Balaton Highland Volcanic Field, Hungary. Central Eur. J. Geosci. 2 (3), 362–384.

Kereszturi, G., Németh, K., Csillag, G., Balogh, K., Kovács, J., 2011. The role of external environmental factors in changing eruption styles of monogenetic volcanoes in a Mio/Pleistocene continental volcanic field in western Hungary. J. Volcanol. Geotherm. Res. 201 (1-4), 227–240.

Kiss, J., Vértesy, L., Gulyás, Á., 2017. Földmágneses esettanulmányok a Balatonfelvidékről, a Duna-Tisza közéről és a Tokaji-hegység területéről. Magyar Geofizika 57 (4), 126–151 (in Hungarian).

Klébesz, R., Gráczer, Z., Szanyi, G., Liptai, N., Kovács, I., Patkó, L., Pintér, Z., Falus, G., Wesztergom, V., Szabó, C., 2015. Constraints on the thickness and seismic properties of the lithosphere in an extensional setting (Nógrád-Gömör Volcanic Field, Northern Pannonian Basin). Acta Geod. Geophys. 50 (2), 133–149.

Koptev, A., Cloetingh, S., Burov, E., François, T., Gerya, T., 2017. Long-distance impact of Iceland plume on Norway's rifted margin. Sci. Rep. 7 (1), 10408.

Kováč, M., Král, J., Márton, E., Plašienka, D., Uher, P., 1994. Alpine uplift history of the Central Western Carpathians: geochronological, paleomagnetic, sedimentary and structural data. Geol. Carpath. 45 (2), 83–96.

Kovács, I., Zajacz, Z., Szabó, C., 2004. Type-II xenoliths and related metasomatism from the Nógrád-Gömör Volcanic Field, Carpathian-Pannonian region (northern Hungary–southern Slovakia). Tectonophysics 393 (1-4), 139–161.

Kovács, I., Green, D.H., Rosenthal, A., Hermann, J., O'Neill, H.S.C., Hibberson, W.O., Udvardi, B., 2012a. An experimental study of water in nominally anhydrous minerals in the upper mantle near the water-saturated solidus. J. Petrol. 53 (10), 2067–2093.

Kovács, I., Falus, G., Stuart, G., Hidas, K., Szabó, C., Flower, M.F.J., Hegedűs, E., Posgay, K., Zilahi-Sebess, L., 2012b. Seismic anisotropy and deformation patterns in upper mantle xenoliths from the central Carpathian–Pannonian region: Asthenospheric flow as a driving force for Cenozoic extension and extrusion? Tectonophysics 514, 168–179.

Kovács, I., Demény, A., Czuppon, G., Lécuyer, C., Fourel, F., Xia, Q.K., Liu, J., Pintér, Z., Király, E., Török, K., Szabó, Á., 2016. Water concentrations and hydrogen isotope compositions of alkaline basalt-hosted clinopyroxene megacrysts and amphibole clinopyroxenites: The role of structural hydroxyl groups and molecular water. Contrib. Mineral. Petrol. 171 (5), 38.

Kovács, I., Lenkey, L., Green, D.H., Fancsik, T., Falus, G., Kiss, J., Orosz, L., Angyal, J., Vikor, Z., 2017. The role of pargasitic amphibole in the formation of major geophysical discontinuities in the shallow upper mantle. Acta Geod. Geophys. 52 (2), 183–204.

Kuritani, T., Xia, Q.K., Kimura, J.I., Liu, J., Shimizu, K., Ushikubo, T., Zhao, D., Nakagawa, M., Yoshimura, S., 2019. Buoyant hydrous mantle plume from the mantle transition zone. Sci. Rep. 9 (1), 6549.

Lambart, S., Baker, M.B., Stolper, E.M., 2016. The role of pyroxenite in basalt genesis: Melt-PX, a melting parameterization for mantle pyroxenites between 0.9 and 5 GPa. J. Geophys. Res. Solid Earth 121 (8), 5708–5735.

Le Roux, V., Dasgupta, R., Lee, C.T., 2011. Mineralogical heterogeneities in the Earth's mantle: constraints from Mn, Co, Ni and Zn partitioning during partial melting. Earth Planet. Sci. Lett. 307 (3-4), 395–408.

Li, Z.X.A., Lee, C.T.A., Peslier, A.H., Lenardic, A., Mackwell, S.J., 2008. Water contents in mantle xenoliths from the Colorado Plateau and vicinity: Implications for the mantle rheology and hydration-induced thinning of continental lithosphere. J. Geophys. Res. Solid Earth 113 (B9).

Liptai, N., Hidas, K., Tommasi, A., Patkó, L., Kovács, I.J., Griffin, W.L., O'Reilly, S.Y., Pearson, N.J., Szabó, C., 2018. Lateral and vertical heterogeneity in the lithospheric mantle at the northern margin of the Pannonian Basin reconstructed from peridotite xenolith microstructures. J. Geophys.Res. Solid Earth 124 (7), 6315–6336.

Liu, J., Xia, Q.K., Deloule, E., Chen, H., Feng, M., 2015. Recycled oceanic crust and marine sediment in the source of alkali basalts in Shandong, eastern China: Evidence from magma water content and oxygen isotopes. J. Geophys. Res. Solid Earth 120 (12), 8281–8303.

Liu, S.C., Xia, Q.K., Choi, S.H., Deloule, E., Li, P., Liu, J., 2016. Continuous supply of recycled Pacific oceanic materials in the source of Cenozoic basalts in SE China: The Zhejiang case. Contrib. Mineral. Petrol. 171 (12), 100.

Lloyd, A.S., Ferriss, E., Ruprecht, P., Hauri, E.H., Jicha, B.R., Plank, T., 2016. An assessment of clinopyroxene as a recorder of magmatic water and magma ascent rate. J. Petrol. 57 (10), 1865–1886.

Mainprice, D., Barruol, G., Ismail, W.B., 2000. The seismic anisotropy of the Earth's mantle: from single crystal to polycrystal. In: Karato, S.-I., Forte, A., Liebermann, R., Masters, G., Stixrude, L. (Eds.), Earth's Deep Interior: Mineral physics and tomography from the atomic to the global scale. 117, pp. 237–264.

Martin, U., Németh, K., 2004. Mio/Pliocene phreatomagmatic volcanism in the western Pannonian Basin. Geol. Hung. Ser. Geol. 26, 1–198.

Márton, E., Fodor, L., 2003. Tertiary paleomagnetic results and structural analysis from the Transdanubian Range (Hungary): rotational disintegration of the Alcapa unit. Tectonophysics 363 (3-4), 201–224.

Matenco, L., Bertotti, G., Cloetingh, S.A.P.L., Dinu, C., 2003. Subsidence analysis and tectonic evolution of the external Carpathian–Moesian Platform region during Neogene times. Sediment. Geol. 156 (1-4), 71–94.

Mazza, S.E., Gazel, E., Bizimis, M., Moucha, R., Béguelin, P., Johnson, E.A., McAleer, R.J., Sobolev, A.V., 2019. Sampling the volatile-rich transition zone beneath Bermuda. Nature 569 (7756), 398.

Mysen, B.O., Boettcher, A.L., 1975. Melting of a hydrous mantle: I. Phase relations of natural peridotite at high pressures and temperatures with controlled activities of water, carbon dioxide, and hydrogen. J. Petrol. 16 (1), 520–548.

Németh, K., Martin, U., Harangi, S., 2001. Miocene phreatomagmatic volcanism at Tihany (Pannonian Basin, Hungary). J. Volcanol. Geotherm. Res. 111 (1-4), 111–135.

Niida, K., Green, D.H., 1999. Stability and chemical composition of pargasitic amphibole in MORB pyrolite under upper mantle conditions. Contrib. Mineral. Petrol. 135 (1), 18–40.

O'Leary, J.A., Gaetani, G.A., Hauri, E.H., 2010. The effect of tetrahedral Al^{3+} on the partitioning of water between clinopyroxene and silicate melt. Earth Planet. Sci. Lett. 297 (1-2), 111–120.

Oszczypko, N., 1992. Late Cretaceous through Paleogene evolution of Magura basin. Geol. Carpath. 43 (6), 333–338.

Patkó, L., Liptai, N., Kovács, I.J., Aradi, L.E., Xia, Q.K., Ingrin, J., Mihály, J., O'Reilly, S.Y., Griffin, W.L., Wesztergom, V., Szabó, C., 2019. Extremely low structural hydroxyl contents in upper mantle xenoliths from the Nógrád-Gömör Volcanic Field (northern Pannonian Basin): Geodynamic implications and the role of post-eruptive re-equilibration. Chem. Geol. 507, 23–41.

Pearson, D.G., Brenker, F.E., Nestola, F., McNeill, J., Nasdala, L., Hutchison, M.T., Matveev, S., Mather, K., Silversmit, G., Schmitz, S., Vekemans, B., 2014. Hydrous mantle transition zone indicated by ringwoodite included within diamond. Nature 507 (7491), 221.

Pécskay, Z., Lexa, J., Szakács, A., Seghedi, I., Balogh, K., Konecny, V., Zelenka, T., Kovacs, M., Poka, T., Fülöp, A., Márton, E., 2006. Geochronology of Neogene magmatism in the Carpathian arc and intra-Carpathian area. Geol. Carpath. 57 (6), 511–530.

Peslier, A.H., Luhr, J.F., 2006. Hydrogen loss from olivines in mantle xenoliths from Simcoe (USA) and Mexico: Mafic alkalic magma ascent rates and water budget of the subcontinental lithosphere. Earth Planet. Sci. Lett. 242 (3-4), 302–319.

Peslier, A.H., Schönbächler, M., Busemann, H., Karato, S.I., 2017. Water in the Earth's interior: Distribution and origin. Space Sci. Rev. 212 (1-2), 743–810.

Pintér, Z., Patkó, L., Djoukam, J.F.T., Kovács, I., Tchouankoue, J.P., Falus, G., Konc, Z., Tommasi, A., Barou, F., Mihály, J., Németh, C., 2015. Characterization of the subcontinental lithospheric mantle beneath the Cameroon volcanic line inferred from alkaline basalt hosted peridotite xenoliths from Barombi Mbo and Nyos Lakes. J. Afr. Earth Sci. 111, 170–193.

Qorbani, E., Bokelmann, G., Kovács, I., Horváth, F., Falus, G., 2016. Deformation in the asthenospheric mantle beneath the Carpathian-Pannonian Region. J. Geophys. Res. Solid Earth 121 (9), 6644–6657.

Ritter, J.R., Christensen, U.R., 2007. Mantle Plumes. Springer-Verlag, Berlin Heidelberg.

Rosenthal, A., Yaxley, G.M., Green, D.H., Hermann, J., Kovács, I., Spandler, C., 2014. Continuous eclogite melting and variable refertilisation in upwelling heterogeneous mantle. Sci. Rep. 4, 6099.

Saal, A.E., Hauri, E.H., Langmuir, C.H., Perfit, M.R., 2002. Vapour undersaturation in primitive mid-ocean-ridge basalt and the volatile content of Earth's upper mantle. Nature 419 (6906), 451.

Schmid, S.M., Fügenschuh, B., Kissling, E., Schuster, R., 2004. Tectonic map and overall architecture of the Alpine orogen. Eclogae Geol. Helv. 97 (1), 93–117.

Schmid, S.M., Bernoulli, D., Fügenschuh, B., Matenco, L., Schefer, S., Schuster, R., Tischler, M., Ustaszewski, K., 2008. The Alps-Carpathians-Dinarides-connection: A correlation of tectonic units. Swiss J. Geosci. 101 (1), 139–183.

Seghedi, I., Downes, H., Vaselli, O., Szakács, A., Balogh, K., Pécskay, Z., 2004. Post-collisional Tertiary–Quaternary mafic alkalic magmatism in the Carpathian–Pannonian region: A review. Tectonophysics 393 (1-4), 43–62.

Seghedi, I., Popa, R.G., Panaiotu, C.G., Szakács, A., Pécskay, Z., 2016. Short-lived eruptive episodes during the construction of a Na-alkalic basaltic field (Perşani Mountains, SE Transylvania, Romania). Bull. Volcanol. 78 (10), 69.

Sobolev, A.V., Shimizu, N., 1992. Ultradepleted melts and the permeability of the oceanic mantle. Dokl. Ross. Akad. Nauk 326, 354–360.

Stephenson, R.A., Berkel, J.T.V., Cloetingh, S.A., 1992. Relation between salt diapirism and the tectonic history of the Sverdrup Basin, Arctic Canada. Can. J. Earth Sci. 29 (12), 2695–2705.

Sundvall, R., Stalder, R., 2011. Water in upper mantle pyroxene megacrysts and xenocrysts: A survey study. Am. Mineral. 96 (8-9), 1215–1227.

Szabó, C., Taylor, L.A., 1994. Mantle petrology and geochemistry beneath the Nógrád-Gömör volcanic field, Carpathian-Pannonian region. Int. Geol. Rev. 36 (4), 328–358.

Szabó, C., Harangi, S., Csontos, L., 1992. Review of Neogene and Quaternary volcanism of the Carpathian-Pannonian region. Tectonophysics 208 (1-3), 243–256.

Szabó, C., Falus, G., Zajacz, Z., Kovács, I., Bali, E., 2004. Composition and evolution of lithosphere beneath the Carpathian–Pannonian Region: A review. Tectonophysics 393 (1-4), 119–137.

Szabó, C., Kovács, I., Dégi, J., Kóthay, K., Török, K., Hidas, K.K., Kónya, P., 2010. From maars to lava lakes: Ultramafic and granulite xenoliths associated with the alkaline basaltic volcanism of the Pannonian Basin. Acta Mineralogica Petrographica Field Guide Series, pp. 1–32.
Szakács, A., Pécskay, Z., Gál, Á., 2018. Patterns and trends of time–space evolution of Neogene volcanism in the Carpathian–Pannonian region: a review. Acta Geodaetica et Geophysica 53 (3), 347–367.
Tari, G., Dövényi, P., Dunkl, I., Horváth, F., Lenkey, L., Stefanescu, M., Szafián, P., Tóth, T., 1999. Lithospheric structure of the Pannonian basin derived from seismic, gravity and geothermal data. Geol. Soc. Lond. Spec. Publ. 156 (1), 215–250.
Tašárová, A., Afonso, J.C., Bielik, M., Götze, H.J., Hók, J., 2009. The lithospheric structure of the Western Carpathian–Pannonian Basin region based on the CELEBRATION 2000 seismic experiment and gravity modelling. Tectonophysics 475 (3-4), 454–469.
Tenner, T.J., Hirschmann, M.M., Withers, A.C., Hervig, R.L., 2009. Hydrogen partitioning between nominally anhydrous upper mantle minerals and melt between 3 and 5 GPa and applications to hydrous peridotite partial melting. Chem. Geol. 262 (1-2), 42–56.
Tollan, P.M., Smith, R., O'Neill, H.S.C., Hermann, J., 2017. The responses of the four main substitution mechanisms of H in olivine to H 2 O activity at 1050° C and 3 GPa. Progress in Earth and Planetary Science 4 (1), 14.
Tommasi, A., Tikoff, B., Vauchez, A., 1999. Upper mantle tectonics: Three-dimensional deformation, olivine crystallographic fabrics and seismic properties. Earth Planet. Sci. Lett. 168 (1-2), 173–186.
Vauchez, A., Tommasi, A., Mainprice, D., 2012. Faults (shear zones) in the Earth's mantle. Tectonophysics 558, 1–27.
Visnovitz, F., Hegyi, B., Balázs, A., Raveloson, A., Rozman, G., Lenkey, L., Lenkey-Bőgér, Á., Király, Á., Pethe, M., Kudó, I., 2018. Mágneses mérések a Balatonon: Észlelt anomáliák és az eredmények értelmezése. Magyar Geofizika 59 (3), 117–128 (in Hungarian with English abstract).
Wang, X.C., Wilde, S.A., Li, Q.L., Yang, Y.N., 2015. Continental flood basalts derived from the hydrous mantle transition zone. Nat. Commun. 6, 7700.
Wéber, Z., 2002. Imaging Pn velocities beneath the Pannonian basin. Phys. Earth Planet. In. 129 (3-4), 283–300.
Wéber, Z., 2018. Probabilistic joint inversion of waveforms and polarity data for double-couple focal mechanisms of local earthquakes. Geophys. J. Int. 213 (3), 1586–1598.
Weis, F.A., Skogby, H., Troll, V.R., Deegan, F.M., Dahren, B., 2015. Magmatic water contents determined through clinopyroxene: Examples from the Western Canary Islands, Spain. Geochem. Geophys. Geosyst. 16 (7), 2127–2146.
Wijbrans, J., Németh, K., Martin, U., Balogh, K., 2007. 40Ar/39Ar geochronology of Neogene phreatomagmatic volcanism in the western Pannonian Basin, Hungary. J. Volcanol. Geotherm. Res. 164 (4), 193–204.
Wilson, M., Downes, H., 2006. Tertiary-Quaternary intra-plate magmatism in Europe and its relationship to mantle dynamics. Geol. Soc. Lond. Mem. 32 (1), 147–166.
Xia, Q.K., Liu, J., Liu, S.C., Kovacs, I., Feng, M., Dang, L., 2013. High water content in Mesozoic primitive basalts of the North China Craton and implications on the destruction of cratonic mantle lithosphere. Earth Planet. Sci. Lett. 361, 85–97.
Xia, Q.K., Liu, J., Kovács, I., Hao, Y.T., Li, P., Yang, X.Z., Chen, H., Sheng, Y.M., 2019. Water in the upper mantle and deep crust of eastern China: Concentration, distribution and implications. Natl. Sci. Rev. 6 (1), 125–144.
Zajacz, Z., Kovács, I., Szabó, C., Halter, W., Pettke, T., 2007. Evolution of mafic alkaline melts crystallized in the uppermost lithospheric mantle: A melt inclusion study of olivine-clinopyroxenite xenoliths, northern Hungary. J. Petrol. 48 (5), 853–883.